Rapeseed mapping using machine learning methods and Sentinel-1 time series coupled with growing degree-days information

Sami Najem, Nicolas Baghdadi, Ya Gao, Hassan Bazzi, Saeideh Maleki, Cassio Fraga Dantas, Dino Ienco

Science of Remote Sensing 11 (2025) 100244

Contents lists available at ScienceDirect

Science of Remote Sensing

journal homepage: www.sciencedirect.com/journal/science-of-remote-sensing

Rapeseed mapping using machine learning methods and Sentinel-1 time series coupled with growing degree-days information

Sami Najem [a,*], Nicolas Baghdadi [a], Ya Gao [b], Hassan Bazzi [c], Saeideh Maleki [a], Cassio Fraga Dantas [a], Dino Ienco [a]

[a] TETIS, Université de Montpellier, CIRAD/CNRS/INRAE, 34093, Montpellier, France
[b] National Space Science Center, Chinese Academy of Sciences, Jingmi North 2nd St, Huairou District, Beijing, 101407, China
[c] AgroParisTech Institut des Sciences et Industries du Vivant et de L'environnement, Paris, France

ARTICLE INFO

Generally, $i = 0$ (the starting date) is the sowing date of the crop. However, given that the sowing date of each plot is not known from the ground truth data, two starting dates were used in this study. For unaligned series, the starting date of GDD accumulation was set as 1 September of the first year in the growing season (approximate date of seed emergence of rapeseed). Whereas, for aligned datasets, the starting date of GDD accumulation was determined based on the detected flowering dates in each dataset.

Keywords:
Rapeseed
Sentinel-1
Growing degree days
Random forest
Inception time

ABSTRACT

In light of recent escalations of geopolitical conflicts around the world, mapping rapeseed areas has garnered great interest given its importance to food security. Sentinel-1 (S1) SAR data was used for timely and regular rapeseed mapping. By coupling S1 data with GDD (Growing Degree Days) information, S1 GDD series were also created and assessed. Rapeseed classification was realized using random forest (RF) and inception time (IT). An alignment method based on detected flowering dates was proposed with the aim of alleviating the possible shifts in he growth cycle between the different sites and years. The spatial (cross-regional) transferability of the models was tested accordingly, before and after alignment. The results showed that using the S1 time series before alignment, the overall F1-score achieved by RF was 81.3 % ± 16.5 %, and the overall F1-score of IT was 89.2 % ± 5.7 %. After alignment, RF achieved an overall F1-score of 90.3 % ± 8.2 %, while the overall F1-score of IT was 91.7 % ± 3.8 %. Using the S1 GDD series, before alignment, the overall score of RF was 58.2 % ± 36.8 %, while the overall F1-score achieved by IT was 86.6 % ± 11.7 %. After the alignment of the S1 GDD series, the F1-score achieved by RF was 73.9 % ± 29.0 %, and the F1-score of IT was 86.8 % ± 10.3. The best configuration for rapeseed mapping was using IT with S1 time series after alignment, as it gave the highest overall F1-score and the best consistency with the lowest standard deviation. Overall, the S1 time series provided better results than the S1 GDD series, meaning that employing thermal time does not enhance the classification performance. The results indicate that the proposed method enables reliable, timely and continuous rapeseed monitoring, Paving the way for more effective food stock management and planning by policymakers and stakeholders.

1. Introduction

The unprecedented growth of the global population has resulted in a continuous rise in food demand and the intensification of agricultural production (Meyfroidt, 2018; Bindraban et al., 2012; Rondanini et al., 2012). Rapeseed is a strategic crop when it comes to food security. It is one of the most important seed oil crops in the world (Friedt et al., 2018). It is also used as a protein source and as food for livestock (Rondanini et al., 2012; Girault, 1973). Rapeseed is also used to produce renewable biofuels (Van Duren et al., 2015). According to many studies, rapeseed cultivation experienced a significant surge starting in the mid-twentieth century (Rondanini et al., 2012; Mittaine and Mielke, 2012). Due to the importance of rapeseed, accurate and up-to-date data on rapeseed cultivation areas holds great significance for agricultural planning, as well as ensuring food and energy stability and promoting environmental sustainability (Luo et al., 2022; Bajželj et al., 2014).

Agricultural monitoring systems using remote sensing data were developed in many countries (Remote Sensing of Land Resources, 2015; Mulla, 2013). The recent increase in the availability of open-source satellite imagery has afforded new opportunities for cropland monitoring. The latest open, freely available data from the Sentinel-1 ("S1", Synthetic Aperture Radar in C-band) and the Sentinel-2 ("S2", optical sensor) constellations offer an opportunity for regular and detailed crop monitoring, because they offer high temporal frequency. S1 has an optimal revisit time of 6 days before January 2022 and 12 days January 2022 onwards) and S2 has an optimal revisit time of 5 days. Furthermore, these constellations offer high spatial resolution (S1 bands: 10 m. S2 bands: 10, 20, or 60 m), allowing for earth surface monitoring at very

* Corresponding author.
E-mail address: sami.najem@inrae.fr (S. Najem).

https://doi.org/10.1016/j.srs.2025.100244
Received 30 October 2024; Received in revised form 19 May 2025; Accepted 31 May 2025
Available online 9 June 2025

small scales (plot scale).

Optical remote sensing has been used for monitoring vegetation cover. By examining reflected light across different spectral bands, it allows for the extraction of vital information regarding vegetation characteristics and dynamics. Optical remote sensing has many applications in vegetation monitoring (Addabbo et al., 2016; Hussain et al., 2020; Zhang et al., 2018; Han et al., 2021) and in cropland mapping, such as for wheat (TAO et al., 2017), rice (Dong et al., 2016) and rapeseed (Zhang et al., 2022; Ashourloo et al., 2019). Several studies used time series of optical multispectral indices such as LAI and NDVI (Normalized Difference Vegetation Index) in order to detect the different growth stages of rapeseed (Hussain et al., 2020; Zhang et al., 2018, 2022), while other studies (Han et al., 2021; Tian et al., 2022) employed a pixel-based method in order to detect rapeseed flowering over large areas, resulting mapping accuracies ranged from 88.58 % to 98.78 %. However, the main challenge for optical remote sensing data is that they are greatly affected by atmospheric conditions, especially cloud cover (Wei et al., 2020), which impedes optical monitoring during long stretches of the year in the northern hemisphere so in some cases optical data may not be available for use (Whitcraft et al., 2015). For these reason, this paper will develop a rapeseed mapping approach that does not use optical data.

This limitation can be overcome with the use of Synthetic aperture radar (SAR) technology. In contrast to optical remote sensing methods, radar utilizes microwave wavelengths, which are capable of penetrating through cloud cover. SAR technology presents a viable alternative to optical remote sensing for crop monitoring and mapping regardless of weather conditions. Indeed, SAR backscattering signal is sensitive to the density, the geometric structure, and to the components of the vegetation (such as leaves, stems, and fruit). This establishes a direct connection between the vegetation cover and the SAR backscattering mechanisms (Jiao et al., 2010; Betbeder et al., 2014; Vreugdenhil et al., 2018; Choudhury and Chakraborty, 2006), leading to its use for crop monitoring and classification in several studies for crops such as wheat (Nasrallah et al., 2019; Kumar et al., 2018), rice (Aschbacher et al., 1995; Nguyen and Wagner, 2017) and others (McNairn and Shang, 2016; Najem et al., 2023; Qadir and Mondal, 2020).

Regarding rapeseed, numerous studies have demonstrated that SAR data can be used for this crop. SAR data has been used for the detection of rapeseed growth stages with good success (McNairn and Shang, 2016; Lampropoulos et al., 2015). When it comes to mapping applications, SAR data has demonstrated abilities in rapeseed mapping, such as in the work of Maleki et al. (2023), who used S1 SAR times series for rapeseed mapping with F1-score between ranging from 86 % to 93 %, and Zhao et al. (2023) who applied a pixel-based rapeseed detection method with resulting F1-scores between 85 % and 95 %, proving the potential of S1 SAR data for rapeseed mapping.

There are many environmental characteristics that affect vegetation development; among these are soil characteristics, light (light intensity and photoperiod) and nutrients. However, temperature is one of the most important environmental factors; it plays a pivotal role in shaping the growth, development, and yield of crops (Qadir et al., 2007; Kaleem et al., 2009; Neild and Newman, 1987; Qian et al., 2019). Fluctuations in maximum and minimum temperatures could affect the growth trajectory of crops. Temperature also plays a role in determining the timing and the duration of certain growth stages. For example through the process of vernalization, which is a characterized by a period of cold temperatures that the rapeseed plant must go through in order to trigger the flowering stage. The effect of temperature on crop growth is best assessed through Growing Degree Days (GDD). GDD serves as a widely adopted heat index for evaluating crop development (Neild and Newman, 1987; Qian et al., 2019). It is calculated as the mean ambient temperature minus the threshold temperature required for the crop's survival. This quantification aids in determining the thermal needs for initiating various growth stages of crops (Nwogha, 2014; Vigil et al., 1997). Many studies have shown that the development of rapeseed is linked to accumulated GDDs (Šidlauskas et al., 2015; Akhter et al., 2015; Shaykewich and Bullock, 2020) and the accumulation of GDD starts from the sowing date of the crop (Neild and Newman, 1987; Qian et al., 2019; Nwogha, 2014; Vigil et al., 1997). GDD accumulation has been shown to be linked to the different developmental stages of rapeseed, including the vegetative stages of flowering, seed formation, and maturity (Akhter et al., 2015; Shaykewich and Bullock, 2020). with accumulated GDD being the greatest determining factor in rapeseed development than other factors such as soil parameters (Šidlauskas et al., 2015).

The accumulation of GDD over the growing season can vary significantly depending on location and year due to varying environmental conditions throughout the growing cycle (from emergence to maturity) between sites and years. In fact, the accumulation of GDD governs the maturity of the crop, leading to differences in the pace of development of a given crop for two different sites or growing seasons. This shift would present itself as a shift in the onset of the developmental stages for the given crop (ex: the flowering stage of rapeseed can start earlier or later between two different locations depending on accumulated GDD). This shift could impair the performance of the classifiers and limit the accuracy of rapeseed mapping. Since GDD is a measure of thermal time, consequently, when S1 data are coupled with GDD information, the result is a representation of the S1 data in function of thermal time, instead of calendar time (radar backscattering coefficients σ° as a function of GDD not as a function of the date, called S1 GDD series hereafter). Thermal time offers the potential to mitigate the impact of possible shifts in timing from one growing season or site to another by accounting for these differences in the rate of accumulation of GDD between different locations and years (Atwell, 1999).

Machine learning techniques are widely used for crop classification (Maleki et al., 2023; Neetu and Ray, 2019; Zhao et al., 2019). Rapeseed mapping was performed using machine learning methods in many studies with good results (Maleki et al., 2023, 2024; Meng et al., 2020). Unfortunately, most studies rely on previously collected terrain data at the same study site and year (Zhang et al., 2022; Liu et al., 2024) or at the same site but in different years (Maleki et al., 2024). However, using different sites for training and testing requires more careful consideration, since in many cases, there are significant time shift in the rapeseed life cycle between study sites in different climates. This limits the spatio-temporal generalization ability for consistent and timely mapping across many sites and many years.

The objective of this study is to enable timely and regular rapeseed mapping using S1 data and GDD information, using the random forest (RF) and inception time (IT) algorithms, without requiring additional a priori data such as crop information (crop type/variety) or the sowing and flowering dates of each field. In order to do that, the paper proposes an approach for aligning the S1 time series of training and test datasets in order to improve the spatiotemporal transferability of classification models (training on one site and testing on another). This alignment is based on detecting the flowering dates for each training and testing dataset. The starting date for the S1 time series and for the calculation of accumulated GDD for the S1 GDD series was set as three months before the detected flowering date. The classification accuracy is assessed using different sites in France and three growing seasons. The results obtained with GDD (S1 series as a function of GDD) are compared to those obtained using the original data (S1 series as a function of S1 acquisition dates).

2. Materials and methods

2.1. Study sites

This study was conducted over three sites in France. The country produces 21 % of the total rapeseed in the European Union (EU) (Oilseeds, 2023). Rapeseed is the EU's major oilseed, accounting for around 60 % of total oilseed production. In terms of quantity (in metric

tons), France produced 4.98 million tons of rapeseed in 2018, 3.52 million tons in 2019, and 3.30 million tons in 2020.

The three sites selected are spread from the north-west to the south-west of France. These sites are Le Mans, La Rochelle, and Tarbes. The Le Mans site is located in the north-west of France in the Sarthe department, near the city of Le Mans, and is approximately 50 km by 50 km in size. The most common crop types on this site are wheat, rapeseed, and barley. The La Rochelle site is located in the Charente-Maritime department in western France, near the city of La Rochelle and is approximately 80 km by 70 km in size. The most common crop types in this site are wheat, corn, and sunflower. Lastly, the Tarbes study site is located in the Hautes-Pyrénées department near the town of Tarbes and is approximately 50 km by 50 km in size. The most common crop types on this site are corn, soy, and sunflower. The two sites of Le Mans and La Rochelle are characterized by an oceanic climate, while the.

Tarbes site belongs to the semi-oceanic climatic zone. Fig. 1 shows the location of the three study sites. For each site, three growing seasons were examined, namely the 2018, 2019, and 2020 growing seasons. The growing season of rapeseed in France normally stretches from August of year 1 to July of year 2, with germination beginning in August, followed by the emergence of the plants and leaf development starting around September of year 1 and persisting until April of the following year. Then comes the budding phase, occurring around April of year 2, followed by the flowering phase starting in May of year 2. Pod formation occurs in May and June, followed finally by the ripening phase that occurs in June and July. Slight yearly variations in this cycle could be observed in response to the different meteorological conditions between the years.

2.2. Ground truth and field boundary data

The RPG (French Graphic Parcel Registry) database was used in this study as the source for field boundary information and for ground truth information. This database serves as a collection of agricultural data based on farmer declarations of agricultural parcels across the country and is produced on a yearly basis. It defines the boundaries of each declared agricultural parcel, and it contains information about that field, such as the crop type and the size of each parcel. The RPG can be downloaded through the French state's GeoServices website (https://geoservices.ign.fr/rpg). The corresponding RPG was used for each growing season in our study. Table 1 shows the number of rapeseed fields compared to the total number of agricultural fields in each study site and for each year.

2.3. Datasets

2.3.1. Sentinel-1 data

SAR data from Sentinel-1 (S1) is available in the C-band at a frequency of 5.405 GHz (wavelength of 5.55 cm) and at a pixel spacing of 10 m. Level-1, ground range detected (GRD), was the product used in this study in the VV and VH polarizations. The S1 constellation was composed of two satellites, namely Sentinel-1A (S1A) and Sentinel-1B (S1B), until December 2021, when the mission ended for S1B, leaving S1A as the only operational satellite. The S1 constellation provided acquisitions with a 6-day revisit time before January 2022 and an acquisition every 12 days from January 2022 onwards. S1 data is provided by the European Space Agency (ESA) and can be accessed freely on the data distribution platform (https://browser.dataspace.copernicus.eu). The downloaded S1 data were calibrated using the ESA S1 toolbox. Firstly, a radiometric calibration was applied in order to transform the data from a digital number (DN) into a backscattering coefficient σ in linear units. Secondly, a geometric correction was performed on the S1 acquisitions using a digital elevation model at 30 m from the Shuttle Radar Topography Mission (SRTM) as a topographical reference (https://eospso.

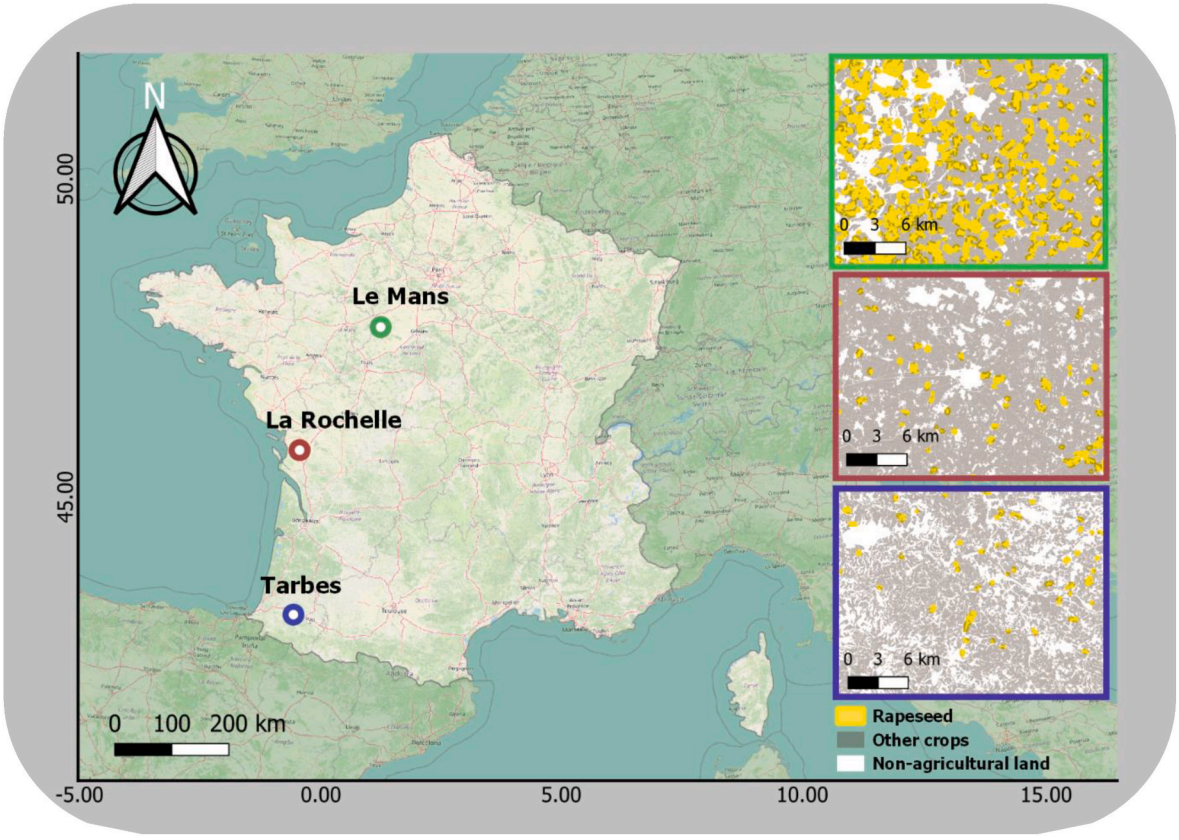

Fig. 1. The location of our three study sites. The Le Mans site is centered around the point: lat = 48.0345, lon = 1.1509, The La Rochelle site is centered around the point: lat = 46.0983, lon = −0.6261, The Tarbes site is centered around the point: lat = 43.3910, lon = −0.7411.

Table 1
Ground truth data used in this study.

Study site	Year	Number of agricultural fields	Number of rapeseed fields	Ratio of rapeseed fields (%)
Le Mans	2018	28602	5291	18.50
	2019	30474	3722	12.21
	2020	29797	4473	15.01
La Rochelle	2018	77649	2639	3.40
	2019	71485	1021	1.43
	2020	96452	1519	1.57
Tarbes	2018	55580	470	0.85
	2019	56105	349	0.62
	2020	56114	371	0.66

nasa.gov/missions/shuttle-radar-topography-mission).

Next, time series for each field in the study area were produced. For every S1 acquisition, the values from the pixels that lie within each field were averaged in order to obtain a single value that represents the average backscattering coefficient over that field at a given S1 acquisition (fields were considered spatially uniform). Finally, these values were then compiled chronologically to form a database containing time series data for all the fields in our study site. These time series were generated for every rapeseed season in our study, namely 2018, 2019, and 2020. Table 2 details the number of S1 images collected across our study sites and the different years.

2.3.2. ERA5 – land dataset

In this study, GDD was calculated using the ERA5-Land dataset. The ERA5 dataset is the fifth generation of ECMWF atmospheric reanalysis produced by Copernicus (Navascues et al.; Quintana Seguí et al., 2016) and is available from 1950 to three months from real-time. Reanalysis utilizes real weather observations as well as modeled data from across the world in order to create a single, consistent, and globally available climatic dataset. It is produced by replaying the land component of the ECMWF ERA5 climate reanalysis. ERA5-Land is based on atmospheric forcing obtained from ERA5's near-surface meteorological conditions and flux parameters. Meteorological conditions are extracted from ERA5's lowest model level (level 137), situated at 10 m above ground level. Downward shortwave, longwave radiation, as well as total precipitation in liquid and solid forms, are the parameters used to interpolate ERA5's original data to ERA5-Land's resolution using a linear interpolation, consequently enhancing the spatial resolution from ~30 km × 30 km (ERA5) to 9 km × 9 km (ERA5-Land).

This data were extracted and downloaded using Google Earth Engine (GEE) (Amani et al., 2020). The ERA5-Land dataset includes 50 variables, among them the hourly 2 m air temperature. This study uses the hourly 2 m air temperature data in order to extract the minimum and maximum air temperatures for each day.

3. Methodology

In this study, from our Sentinel-1 (S1) data, we produced time series, designated hereafter as S1 time series (VV and VH time series with the corresponding S1 acquisition dates), as well as GDD-based series, designated hereafter as S1 GDD series. S1 GDD series are created using S1 data (VV and VH) and the cumulative GDD (ΣGDD) calculated from a starting date, which is generally the assumed date of sowing of the studied crop.

Table 2
S1 dataset used in this study.

Study site	Year	Number of S1 images	Average number of S1 images per month
Le Mans	2018	163	15
	2019	158	14
	2020	168	15
La Rochelle	2018	167	15
	2019	150	14
	2020	164	15
Tarbes	2018	166	15
	2019	155	14
	2020	162	15

Furthermore, seeing that it is possible to have temporal shifts in the rapeseed growth cycle between two different years in the same site (meteorological variations among the years) or between two different study sites (different climatic conditions between the study sites), we proposed an alignment method based on the flowering date of rapeseed that aims to reduce time shifts between the training and testing datasets. This alignment will be used to enhance the classification performance in the case of spatial and temporal transferability of the classification models for S1 time series and for S1 GDD series. Transferability will be tested using different study sites for training and testing.

3.1. Calculation of cumulative GDD

Growing Degree Days (GDD) is a fundamental metric in agricultural and ecological studies, quantifying the accumulated thermal energy available for plant growth on a daily basis. Plant development is intricately linked to temperature. Different species have distinct temperature requirements for growth (Qadir et al., 2007; Kaleem et al., 2009). For a given day (t_i), GDDi is calculated using hourly temperature data from ERA5-Land by summing the daily maximum (Tmax) and daily minimum (Tmin) temperatures, then dividing the sum by 2 and subtracting the base temperature (Tbase) from the result. Tbase represents the minimum temperature threshold below which biological activity is negligible above which, thermal energy starts counting towards GDD calculations. Tbase is essential for predicting plant development accurately since it sets a threshold for temperature. Different species have different Tbase values in the case of rapeseed Tbase was set to 3 °C (degree Celsius) (Luo Tao et al., 2018). The formula of daily GDD (t_i) is expressed as:

$$GDD(ti) = \begin{cases} \frac{Tmax + Tmin}{2} - Tbase & if \ \frac{Tmax + Tmin}{2} > Tbase \\ 0 \quad if \ \frac{Tmax + Tmin}{2} \leq Tbase \end{cases} \quad (1)$$

The cumulative GDD ($\Sigma GDD(t_n)$) provides a measure of thermal time. It is calculated starting at a reference date, usually, sowing date. $\Sigma GDD(t_i)$ is calculated as the sum of $GDD(t_i)$ from the starting date to t_i. Thermal time is a way of quantifying the relationship between temperature and crop development. It measures the cumulative amount of thermal energy that a plant is exposed to over time, usually expressed in degree-days. The advantages of thermal time are mainly limiting the effects of potential temporal shifts from location to location and growing season to growing season. It is also an index for predicting phenological events, such as budding, flowering, and harvesting. The formula for ΣGDD for a given date t_n is expressed as:

$$\Sigma GDD(tn) = \sum_{i=1}^{n} GDD(ti) \quad (2)$$

Fig. 2 shows the accumulated GDD with 1 September as the starting

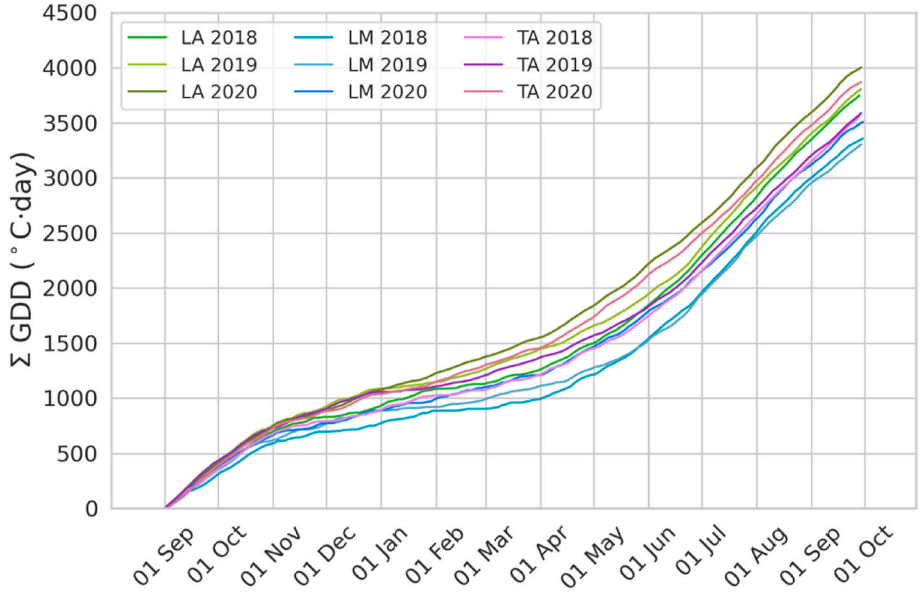

Fig. 2. ΣGDD as a function of time for each site and for each year in our study. LA: LA rochelle, LM: LE mans, TA: tarbes.

date. It shows that for a given site, slight shifts in some cases and significant shifts in others can be observed in the ΣGDD between the different years. Similarly, a weak or strong shift between two years for two distinct sites can be observed. Secondly, we can see that there is a marked increase in cumulative GDD (ΣGDD) during September and October due to elevated temperatures during these months (this is true for all summer months as well). Meanwhile, the increase in ΣGDD remains minimal between November and March, followed by a substantial surge starting in April as temperatures become significantly warmer.

For certain datasets in our study, the disparity between ΣGDD remains unchanged over time, as exemplified by La Rochelle (2020) (LA, 2020) and Tarbes 2020 (TA, 2020). For other datasets, the gap widens over time, up until April, after which it stabilizes, for example, LA 2020 and Le Mans 2018 (LM, 2018). This means that for a given date, ΣGDD could have significantly different corresponding values between two datasets (Fig. 2). For example, for an S1 acquisition on May 1, the shift is approximately 600 (°C.days) between the LM2018 and LA2020 datasets, leading to a significant difference between the time series and the GDD series. On the other hand, we do not see a significant difference between Le Mans 20218 (LM2018) and Le Mans 2019 (LM2019).

3.2. Detection of flowering date

The observed temporal shifts in the rapeseed growth cycle between two different years at the same site or between two different study sites can lead to misclassification, therefore reducing mapping accuracy (Maleki et al., 2023, 2024). For this reason, we proposed to align the training and testing datasets with the aim of alleviating these shifts.

Since the sowing dates are not available in our ground datasets, the calculation of ΣGDD becomes rather approximate, as only one date is chosen for each given dataset rather than one sowing date for each plot. Seeing that the sowing date is difficult to estimate from satellite images, we decided to use the flowering stage as a reference for the starting date. Flowering is a major stage in the life cycle of rapeseed, since it marks the transition from the vegetative phase to the seed production phase. numerous studies have shown the potential of radar images for detecting the flowering stage of rapeseed with very high correlation (r values up to 0.96) (McNairn et al., 2018, 2018d'Andrimont et al., 2020). The flowering date of the rapeseed plant can be identified by a decrease in the SAR signal in VV polarization during the months of April and May in France (McNairn et al., 2018, 2018d'Andrimont et al., 2020). Fig. 3 shows the signature dip in the average S1 time series of rapeseed plots in the VV polarization, marking the flowering stage.

Fig. 4 shows the steps needed for detecting the flowering date. The process is separated into two segments, one for training datasets (Fig. 4a, where we do know the crop type of each field) and one for testing datasets (Fig. 4b, where we do not know the crop type of each field).

3.2.1. A. training datasets

For each of our training datasets, the location of the rapeseed fields is known (using ground truth data, the RPG in our study). In order to detect the flowering date for each reference rapeseed field, we first apply a Gaussian smoothing to the S1 time series for VV polarization (because VV enables us to detect the flowering peak (Han et al., 2021)). Then, we

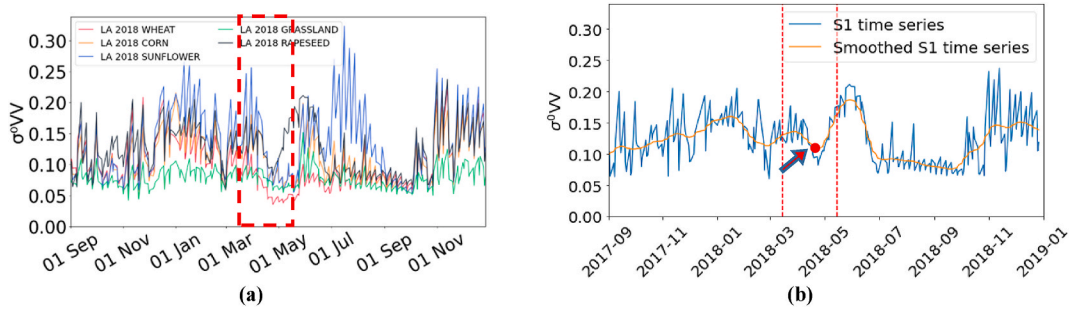

Fig. 3. (a) average S1 time series for the main five crop types, the period from 15 March to 15 May is framed in a red box. (b) flowering date detection (red dot) for one rapeseed field of the training dataset La Rochelle 2018.

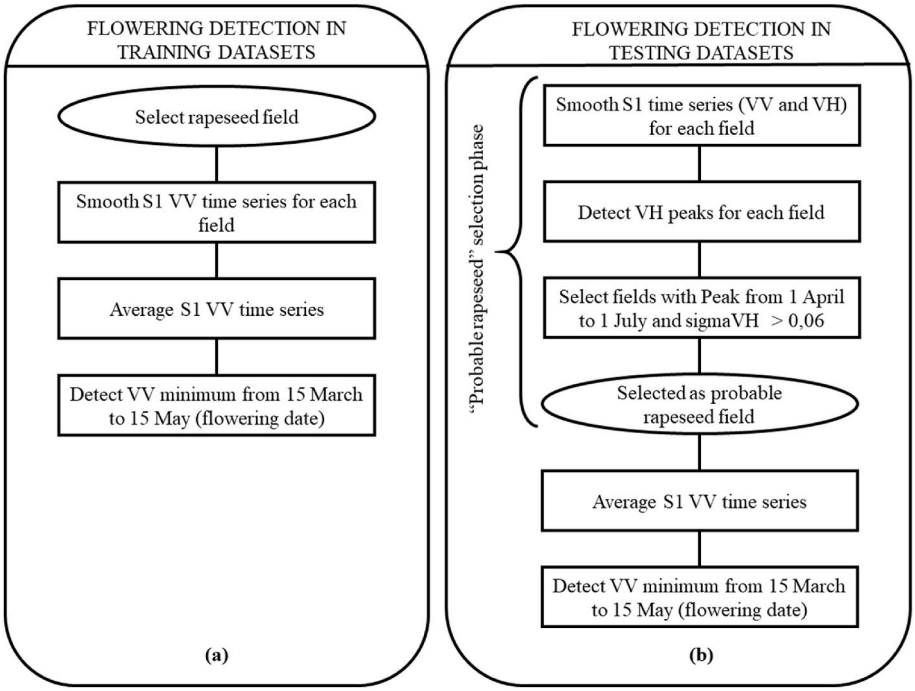

Fig. 4. Flowchart of the detection flowering-date detection. (a) Flowering detection for training datasets. (b) Flowering detection for testing datasets.

calculated the average S1 time series in the VV polarization of all rapeseed fields. Next, using this average time series, we detected the average flowering date by finding the minimum (as seen in Fig. 3a for rapeseed) in the period spanning from 15 March to 15 May. Fig. 3a compares the average S1 time series for rapeseed with those of other crops. The minimum that can be clearly seen in the S1 signal in the VV polarization is indicative of the flowering stage (d'Andrimont et al., 2020). Fig. 3b shows the detected flowering minimum in the smoothed average S1 time series in the VV polarization of rapeseed fields.

3.2.2. B. Testing datasets

Since in the testing datasets we do not have the crop type information, first we will need to identify probable rapeseed fields in order to determine the probable average flowering date for each testing dataset. First, we applied Gaussian smoothing to the S1 time series for both VV and VH polarizations. Next, we looked for a signature increase in the S1 signal in the VH time series from 1 April to 1 July (Maleki et al., 2024; McNairn et al., 2018) which is linked to the pod formation stage in the rapeseed's life cycle. As shown in Fig. 5a, this peak is much greater for rapeseed than for any other type of crop during that period. Therefore, for each field in the dataset, the peaks were detected from the smoothed VH time series. The fields that showed an important peak of more than 0.06 in linear units (>-12 in dB) between 1 April and 1 July were considered probable rapeseed fields, while fields that did not satisfy this condition were not selected. These steps ensure that the selected fields are rapeseed fields with high certainty. Two examples of selected rapeseed fields are shown in Fig. 5b and c, as well as two examples of fields that were not selected as rapeseed fields (Fig. 5d and e) because they do not show a high peak between 1 April and 1 July.

After selecting the probable rapeseed fields, we averaged the S1 time series in the VV polarization of the selected fields. Next, using the average S1 time series in VV polarization, we detected the flowering date for the dataset by finding the minimum in the period spanning from 15 March to 15 May.

3.3. Creating S1 GDD series

As mentioned in the previous section, S1 GDD series are produced from S1 data and GDD information. The process of creating S1 GDD series, shown in Fig. 6, includes two phases, the first is calculating ΣGDD at each S1 acquisition date, and the second is the resampling phase. We begin by calculating ΣGDD, using ERA5-Land data for each of the dates in the S1 time series. Starting from 0 °C.days at day 0, the cumulated of GDD (ΣGDD) was calculated for each S1 date by adding the GDD values from the starting date to the date of each S1 acquisition. Since each day contributes a certain amount of GDD, then replacing the S1 date with the corresponding ΣGDD. The second step in creating S1 GDD series consists of replacing the acquisition dates with their corresponding ΣGDD thus the S1 time series backscattering coefficient at time t becomes the backscattering coefficient at a corresponding ΣGDD. This step assures the transition from a series based on calendar time (dates in this case) to a series based on thermal time (since ΣGDD is a representation of thermal time). As we have seen in Fig. 2, the increase in ΣGDD is not linear throughout the year, with bigger increases occurring during the hotter months of the year. Hence, during the summer months, the increase in ΣGDD between two consecutive S1 dates will be much larger than that during the winter months. Next, resampling was applied in order to regularize the GDD step across all the study sites and years. This part of the process is called the "resampling phase". Initially, the S1 dates were replaced by their corresponding ΣGDD values (ΣGDDi at each date). Next, the x-axis was resampled to one data point every 20 GDDs and the S1 data were consequently resampled at every 20 GDD step.

The starting point is of great importance when calculating ΣGDD. However, operationally, we do not know the real sowing date of every field in our study sites since it is not available as part of the RPG surveys in the ground truth data. Nevertheless, we do know that in France, sowing usually occurs in August and seed emergence occurs in September. We will test two starting points. The first one is September 1 corresponding to the probable emergence date ±15 days (before this date, there is no detectable vegetation activity). The second starting date is based on the detected flowering stage used for alignment of the datasets, discussed in the previous sections.

3.4. Classification algorithms

In this study, rapeseed fields are mapped using RF and IT. The

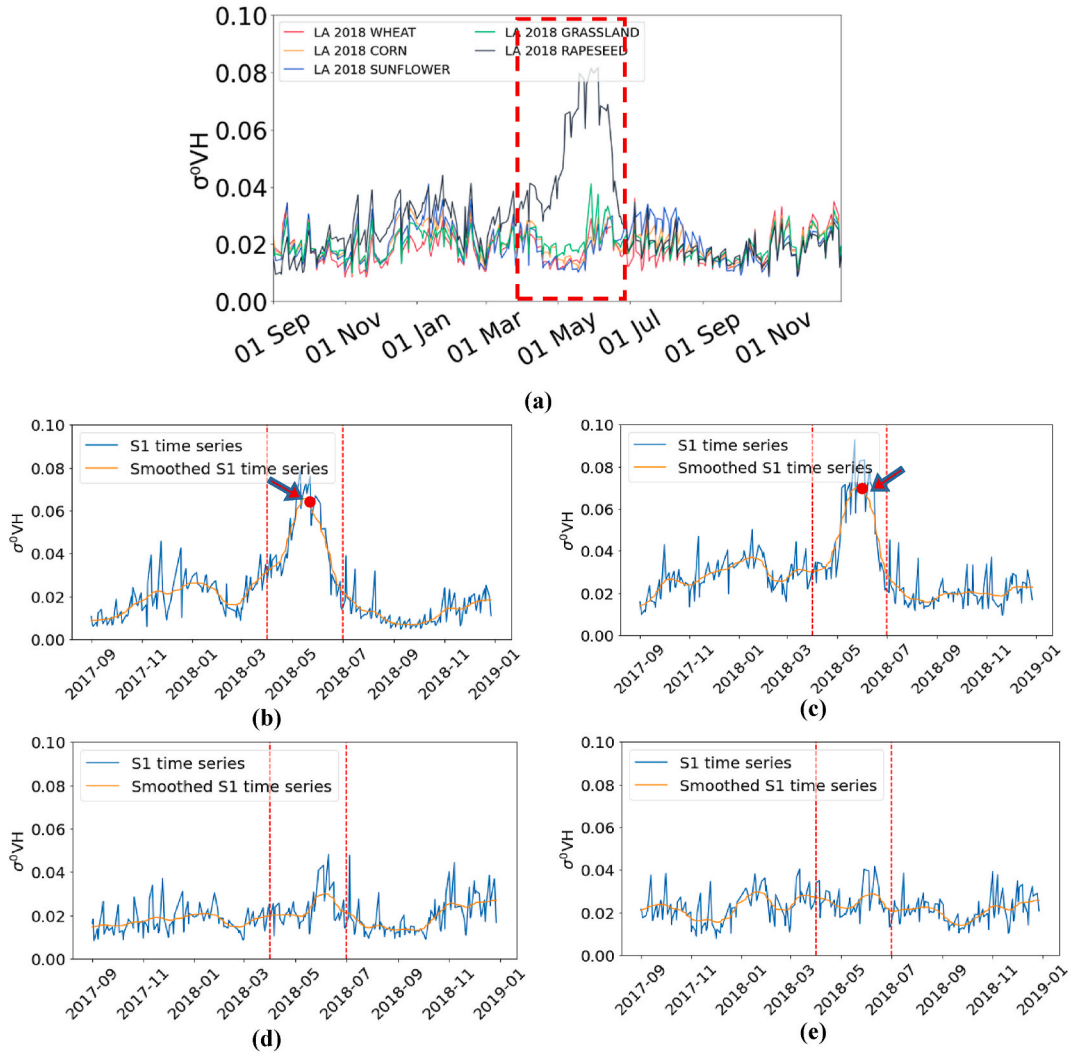

Fig. 5. (a) average S1 time series in La Rochelle (2018) in VH polarization for the five main crop types (red box = period from 1 April to 1 July). (b) and (c) S1 time series as well as the smoothed S1 time series (Gaussian smoothing) for selected (probable rapeseed) fields, the arrow points to the peak detected (red dot) from 1 April to 1 July. (d) wheat field, (e) grassland field, neither of which were selected (no peak over 0.06 from 1 April to 1 July).

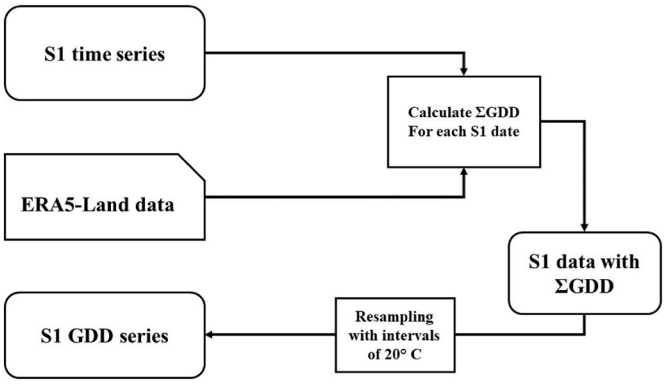

Fig. 6. Production of S1 GDD series datasets.

performance of these two classifiers will be tested before and after alignment. Random forest is an ensemble machine learning technique that combines the outcomes of numerous decision trees to enhance classification accuracy and mitigate overfitting (Inglada et al., 2015). We employed 100 decision trees with default configurations for other parameters. The second machine learning tool used, inception time, is a multivariate time series classification algorithm made up of five distinct deep Convolutional Neural Network (CNN) models augmented with residual connections (Ismail Fawaz et al., 2020). The inception time model was optimized using the Adam optimizer. The parameters used were $\beta 1 = 0.9$, $\beta 2 = 0.999$, $\varepsilon =$ 1e-07, with a learning rate of 1e-5 and a weight decay of 1e-6. Furthermore, we set the batch size to 16, and we used a standard cross-entropy loss function.

We will test all the possible cases of spatiotemporal transfer (training and testing in different sites) using S1 time series and S1 GDD series, first without alignment, then with alignment, resulting in a total of 54 combinations for each database (S1 time series and using S1 GDD series). We will begin the first phase of the investigation by evaluating the transferability of our two classifiers before alignment, using the complete S1 time series and using 1 September as a starting date in ΣGDD calculation for the S1 GDD series. In the second phase of the investigation, we will evaluate the spatiotemporal transferability of our classifiers using each database after alignment.

To assess the classification results, we employed a range of accuracy measures. These metrics include recall, precision, F1 score, and Kappa. The formulas for each are available in Table 3.

Table 3
Metrics used in this study. With TP: True positives, TN: True Negatives FN: False Negatives, FP: False positives.

Metric	Equation
Recall	$\frac{TP}{TP+FN}$
Precision	$\frac{TP}{TP+FP}$
F1-score	$\frac{2*(Precision*Recall)}{Precision+Recall}$
Kappa	$\frac{2*((TP*TN)-(FN*FP))}{(TP+FP)*(FP+TN)+(TP+FN)*(FN+TN)}$

4. Results

4.1. Resulting S1 GDD series

Fig. 7a shows the original time series (S1 time series) for the La Rochelle study site for the 2018, 2019, and 2020 growing seasons. We can see that the rapeseed crop shows the distinctive flowering dip in March/April, followed by a very strong increase in the signal in June/May. Fig. 7b shows the S1 GDD series for the La Rochelle study site for the 2018, 2019, and 2020 growing seasons that resulted from the S1 GDD series creation process (S1 data as a function of ΣGDD).

4.2. Aligned S1 time series and S1 GDD series

In this study, we proposed an alignment of the training and testing datasets based on the flowering date. In fact, flowering is a major stage in the life cycle of rapeseed. Its success guarantees good crop yields come harvest time. Consequently, using the flowering point as a reference, all the datasets in this study will be brought to a common point in their life cycle.

For the aligned S1 time series, the starting date was set to three months before the detected flowering date, which is around the beginning of the vegetative phase and the end date was three months after the detected flowering date, coinciding within the harvest month (1–2 weeks before harvest).

The next step is converting the S1 dates to the number of days since the starting date (day 0 = the starting date corresponding to three months before the flowering date), then resampling the new datasets every five days. This is applied to all the fields in the dataset. As for the S1 GDD series alignment, the starting date for ΣGDD calculation was set three months before the detected flowering date.

Fig. 8 shows an example of the data before and after alignment between two datasets, Le Mans 2019 as a training dataset and Tarbes 2020 as a testing dataset. Fig. 8a (VV) and Fig. 8b (VH) show the trimmed S1 time series of rapeseed fields before alignment (from 3 months before flowering to 3 months after flowering). There is a time shift of around 30 days between the two datasets, with flowering for Le Mans 2019 occurring around the end of May, whereas for Tarbes 2020, it is around the end of April (Fig. 8a). Furthermore, the same shift is seen in the signature rapeseed peak between the two datasets (Fig. 8b). Fig. 8c (VV) and Fig. 8d (VH) show the average S1 time series of rapeseed fields after alignment (day 0 corresponds to three months before flowering date for each dataset). We can see that by aligning the flowering dates of the two datasets (at day 90), the shift has been minimized between the flowering dips as well as the peaks of the two datasets. Fig. 8e (VV) and Fig. 8f (VH) show the S1 GDD series using three months before the flowering as the starting date. We can see that the shift between the two datasets was also reduced.

4.3. Analysis of S1 time series and S1 GDD series

Fig. 9a and b show the average signal of all the rapeseed fields for every dataset (study site/growth season) in VV and VH polarizations using the S1 time series, and Fig. 9c and d use the S1 GDD series. The beginning of September was used as the starting date for both of these series, as it was around the time of seed emergence.

When examining the S1 time series in Fig. 9a and b, a temporal shift between the different datasets is observed. In some cases, it reaches around 1.5 months, as in the case of TB 2020 and LM 2019. On the other hand, shifts are also visible in the S1 GDD series, reaching as high as around 600 GDD (for example, LM, 2018 vs. LA, 2020). This temporal shift between the S1 GDD series is due to factors linked to a difference in the sowing date, the different climatic conditions that could affect vegetation growth (precipitations, temperature), soil type, etc.

Analyzing the results of coupling GDD to S1 data shows four possible cases:

- The first case study where there is no time shift in the S1 time series and no difference in ΣGDD (using Fig. 2 as a reference) between two given datasets, thus the S1 GDD series will have no shift (example: LR, 2018 and TB, 2018).
- The second case study where there is no time shift in the S1 time series between two given datasets but a difference in ΣGDD; in that case, a shift will be introduced in the S1 GDD series (example: LM, 2018 and LR, 2019).
- The third case has a time shift in the S1 time series between two datasets that is corrected in the S1 GDD series (example: LR and TA, 2020 have a shift of around a month in the unaligned S1 time series but no shift in the unaligned S1 GDD series).
- The final case covers a scenario where a time shift in the S1 time series exists and is not corrected in the S1 GDD series (example: LM, 2019 and LR, 2020 have a time shift in the unaligned S1 GDD series and a shift in the unaligned S1 GDD series)

A comparison between the time series of rapeseed and the most common crop types at our study sites is shown in Fig. 10, S1 GDD series can be found in the appendix. The average signal for rapeseed in the VH polarization in the S1 time series has a characteristic peak around the month of May, with sigma VH reaching 0.08 on average (approximately −11 dB, Fig. 10a), whereas the signal for other crops is much lower. On the other hand, in the VV polarization, the rapeseed peak is not as explicitly distinguishable from that of other crops. Furthermore, the characteristic rapeseed peak, corresponding to the pod formation stage, partially overlaps in VV with peaks of corn, grassland, and sunflower.

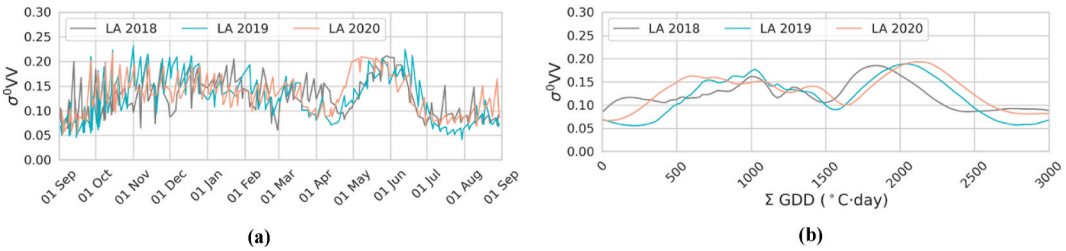

Fig. 7. The two types of series used in this study in for three growing seasons in the La Rochelle site. (a) Average S1 Time series with dates in the x-axis. (b) Average S1 GDD series data with ΣGDD in the x-axis. LA 2018: La Rochelle 2018, LA 2019: La Rochelle 2019, LA 2020: La Rochelle 2020.

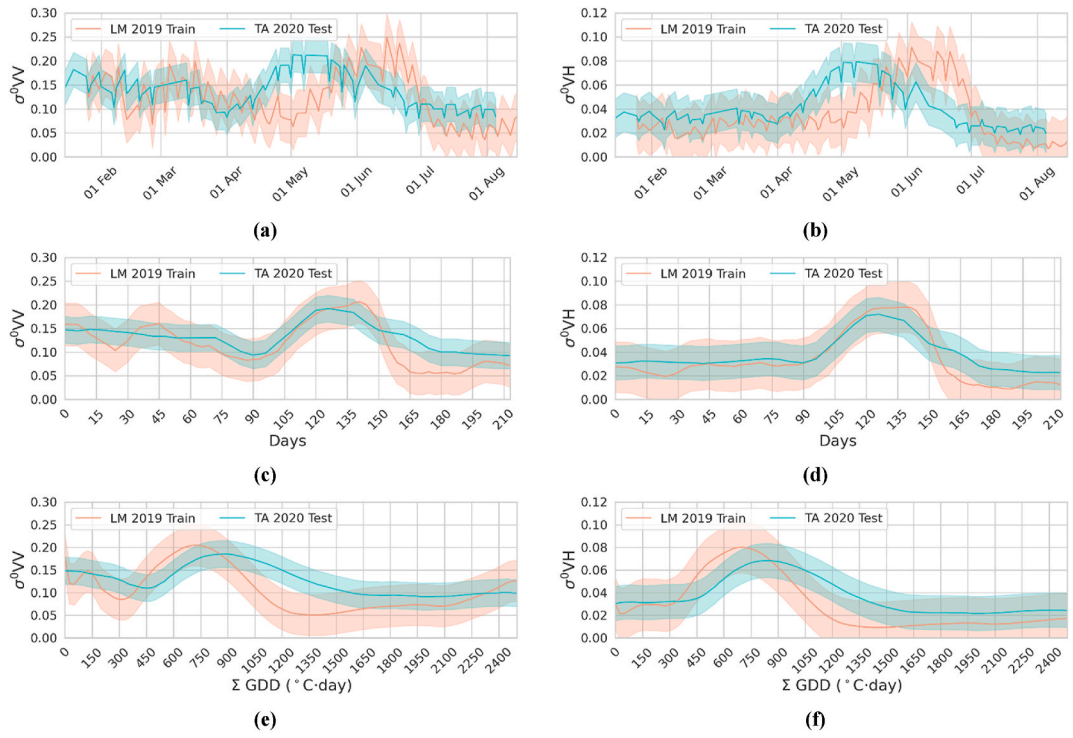

Fig. 8. S1 series before and after alignment with the Le Mans 2019 as the training dataset and Tarbes 2020 as the testing dataset. (a,b): S1 time series (before alignment) (a:VV, b:VH), (c,d): aligned S1 times series (c:VV, d:VH) day 0 in the graph represents 90 days before flowering, (e,f) aligned S1 GDD series (e:VV, f:VH). The shaded area corresponds to the standard deviation.

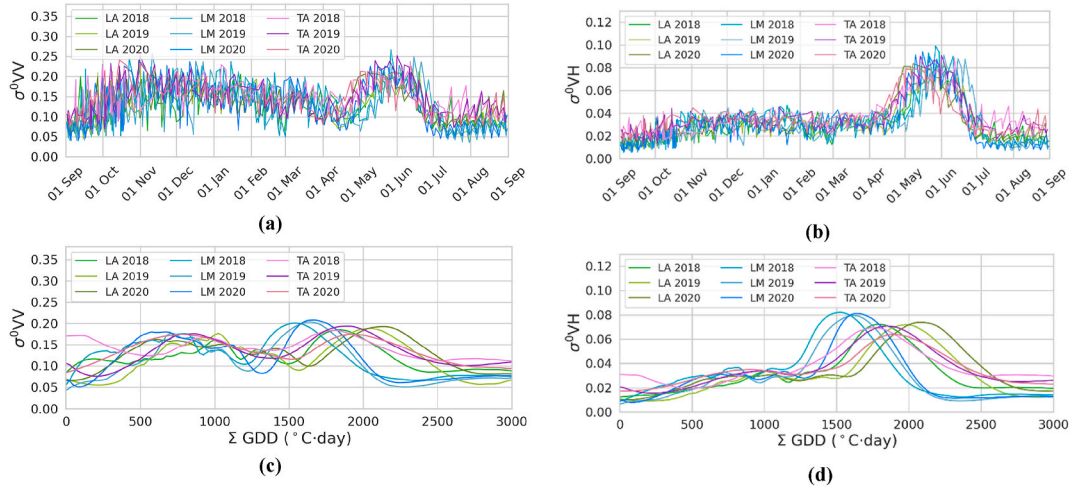

Fig. 9. S1 times series (a and b) and S1 GDD series (c and d) showing the rapeseed averages in σVV and σVH for each dataset (three sites and three growing seasons).

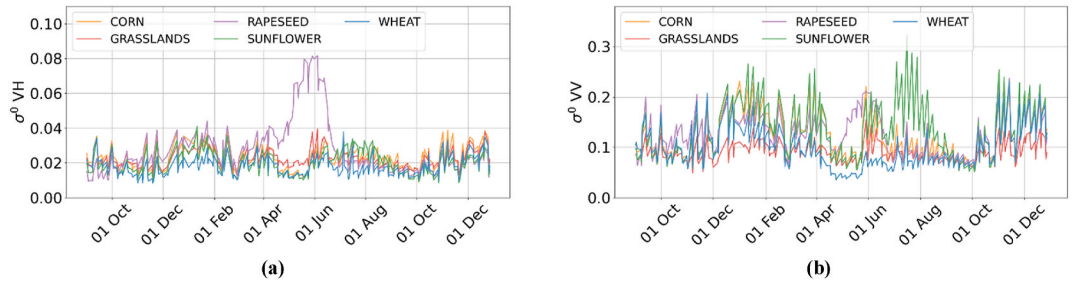

Fig. 10. S1 time series according to S1 acquisition dates showing the main crops in La Rochelle (2018) dataset.

Therefore, VH shows higher potential for rapeseed classification. However, the clear minimum in VV just before the characteristic rapeseed peak is used for identifying the flowering period (Fig. 10b). For example, the flowering period is around mid-April LA 2018.

As for the S1 GDD series (figures found in the appendix), the VH polarization reaffirms its strong potential to classify rapeseed (Fig. 22a). On the other hand, VV (Fig. 22b) shows a lower but non-negligible potential due to the partial overlap observed with sunflower.

4.4. Estimated flowering dates

Our proposed series alignment method is based on detecting the average flowering date for each dataset. The flowering dates were detected by finding the signature rapeseed minimum between 15 March and 15 May. The estimated flowering dates are presented in Table 4 for every same site and year as training or testing. The results were not validated using real flowering date data because that type of data is not widely available, however, Table 4 shows that the flowering dates ranged from 2 April to 26 April, which lies within the expected range of flowering date in France. The estimated flowering date varied up to 18 days between 3 years of the same site, meaning that although photoperiod plays a role in determining the flowering stage of rapeseed, the plants are still greatly impacted by yearly variations of temperatures.

For the testing dataset, the flowering dates ranged between 5 April to 26 April. Comparing the training and testing flowering dates of each dataset, we observe that flowering dates between both datasets are very close to each other, with the biggest difference reaching 4 days, which is less than the revisit time of the S1 constellation (Tarbes, 2018).

4.5. Classification of rapeseed fields

4.5.1. Rapeseed detection using S1 time series before alignment

Firstly, the performance of the two classifiers was examined using the unaligned S1 time series that starts on September 1 (corresponding to the approximate time of seed emergence). The spatiotemporal transferability was assessed using the different sites for training and testing (all possible combinations for each couple of training-testing datasets, for a total of 54 combinations).

Fig. 11 represents the accuracy metrics for the transferability of IT and RF classifiers (results for aligned S1 time series are found in the appendix). The average value of metrics (Mean), the highest (Max) and lowest (Min) values calculated from the IT classifier show that the average F1 scores were consistently above 83.0 %, with the lowest scores never dropping below 70 %. The RF classifier achieved average F1 scores higher than 68.8 %, with the lowest minimum score of 22 %. Kappa values show a similar pattern, with average Kappa values remaining greater than 0.81 and minimums consistently greater than 0.79 for IT. RF did not perform consistently well, with average Kappa values as low as 0.68 and the lowest minimum score reaching 0.22. The average recall scores of IT were always above 80 %, while they were as low as 57.6 % when using RF. Average precision scores were consistently above 78 %, regardless of the classifier used. The worst results corresponded to datasets that had the greatest time shift (F1-score of 22.0 % for Le Mans, 2019 as training and Tarbes, 2020 as testing).

Table 4
Flowering dates for each dataset, with each dataset considered as Training (known rapeseed fields) and Testing (probable rapeseed fields).

Dataset	Training	Testing
La Rochelle 2018	April 22, 2018	April 21, 2018
La Rochelle 2019	April 08, 2019	April 07, 2019
La Rochelle 2020	April 04, 2020	April 04, 2020
Le Mans 2018	April 26, 2018	April 26, 2018
Le Mans 2019	April 23, 2019	April 23, 2019
Le Mans 2020	April 14, 2020	April 14, 2020
Tarbes 2018	April 11, 2018	April 12, 2018
Tarbes 2019	April 02, 2019	April 06, 2019
Tarbes 2020	April 02, 2020	April 05, 2020

4.5.2. Rapeseed detection using S1 GDD series before alignment

Fig. 12 reports the result assessment in the case of spatiotemporal transferability, which was also tested using the unaligned S1 GDD series with 1 September as the starting date (results for aligned S1 GDD series are found in the appendix). For IT, the average F1 scores were consistently above 79 %, while RF achieved average F1 scores as low as 16.7 %, with the lowest minimum achieved score of 0 %. Kappa values with IT were consistently over 0.78, while for RF they dropped to 0.17, with the lowest minimum score reaching 0. The average recall scores for IT ranged between 68.9 % and 95.6 %, whereas for RF, they ranged between 12.5 % and 95.2 %. For IT, the averages of precision were consistently above 78 %, whereas for RF, they ranged between 54.9 % and 98.6 %. The worst result with RF (F1-score of 0 %) corresponded to datasets that had the greatest GDD shift (600 (°C.days) between Le Mans 2018 and La Rochelle 2020).

The S1 GDD series was outperformed by the S1 time series. This is mainly evidenced by the difference of 28 % in the overall F1-score for RF. Furthermore, although IT did not show a significant decrease in the overall F1-score (2 % decrease) when using the S1 GDD series, it showed more fluctuations in the results compared with the S1 time series.

4.5.3. Rapeseed detection after alignment

The biggest challenge for rapeseed mapping is the lack of ground truth data in many regions, as some sites pose greater obstacles for ground truth campaigns. Previous studies have shown that transferring a model trained at a given site between different years at that same site yields very good results (Maleki et al., 2023, 2024). For this reason, this study evaluated the spatiotemporal transferability (transferring a model to a different site) of RF and IT using the S1 time series as well as the S1 GDD series. These results were compared with the results after the application of our proposed alignment method.

Fig. 13 shows the F1-scores of the models in the spatiotemporal transfer scenario using S1 time series, before and after alignment of the training and testing datasets. Fig. 13a and b show the F1-scores of IT before and after alignment. A comparison between IT performance before and after alignment shows a slight overall improvement across all sites and years. Higher improvement is shown for the combinations that performed the worst before alignment. For example, the performance of the combination of LA2020 training and LM2018 testing improved from 70.0 % to 91.4 %. Similarly, the combination of LM2019 and TA2018 as training testing sets, respectively, showed an improvement in the F1-score from 77.5 % before alignment to 91.6 % after alignment. Other combinations showed marginal improvement, such as that for LA2019 as training and all other datasets as testing.

Fig. 13c and d compare the same results before and after alignment of the S1 time series using RF. Contrary to the marginal improvement shown by IT, RF showed significant improvement in the classification performance before and after alignment using the S1 time series data. The average improvement across sites and years reaches 9.0 %, from 81.3 % to 90.3 %. Some combinations showed high improvement, as for LA2020-LM2018, with an F-score improving from 49.6 % to 96.9 % after alignment using RF. Similarly, in the case of TA2018-LM2018, there was an improvement from 35.9 % to 97.8 % in the F1 score. The results improved greatly after alignment, with marked increases in the F1-scores for most combinations of training and testing.

The performance of the two models was also examined before and after the alignment of the S1 GDD series. Fig. 14a and b depict the results of IT before and after the alignment of the training and testing datasets. The results show that for IT, only slight improvements in the F1-scores were obtained after the alignment, whereas the RF classifier did benefit from the alignment, as we can see by the improvement of the F1-scores for most combinations between Fig. 14c and d.

When examining the results of the S1 time series, we see in Table 5

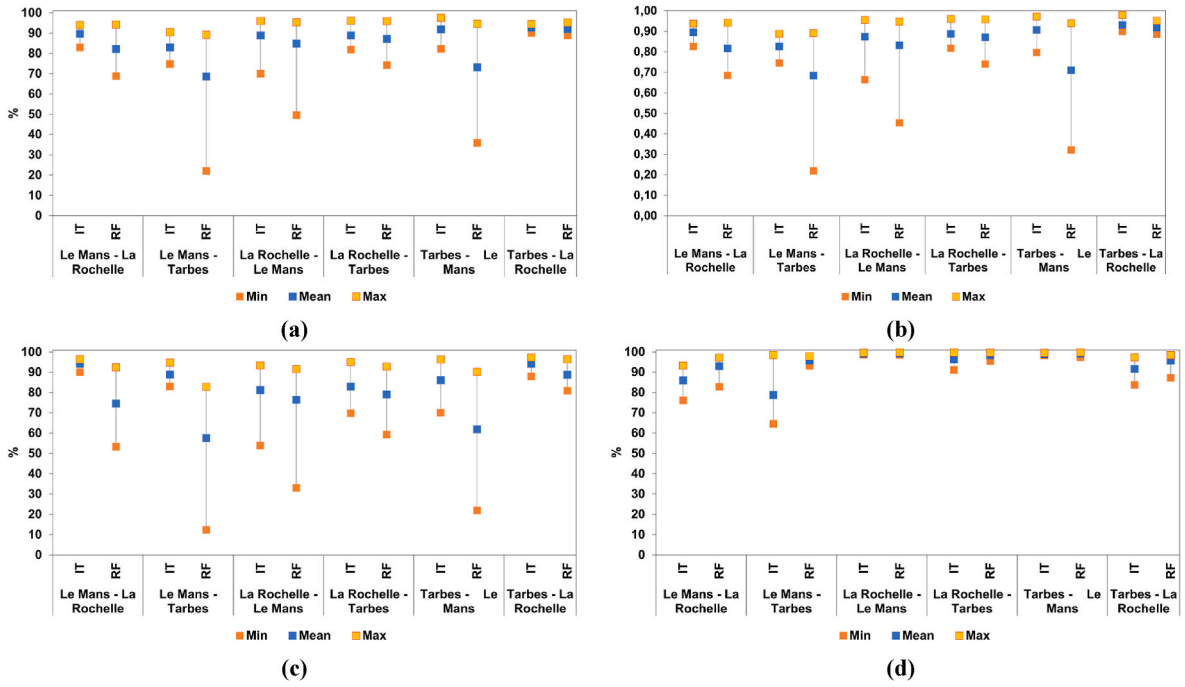

Fig. 11. Accuracy assessment for inception time (IT) and random forest (RF) using the unaligned S1 times series (different site and year for training and testing): (a) F1-Score, (b) Kappa, (c) Recall, (d) Precision. 'Mean' represents the average, 'Max' represents the highest value and 'Min' represents the lowest value of each metric across the possible combinations of sites and years (9 combinations for each couple of datasets).

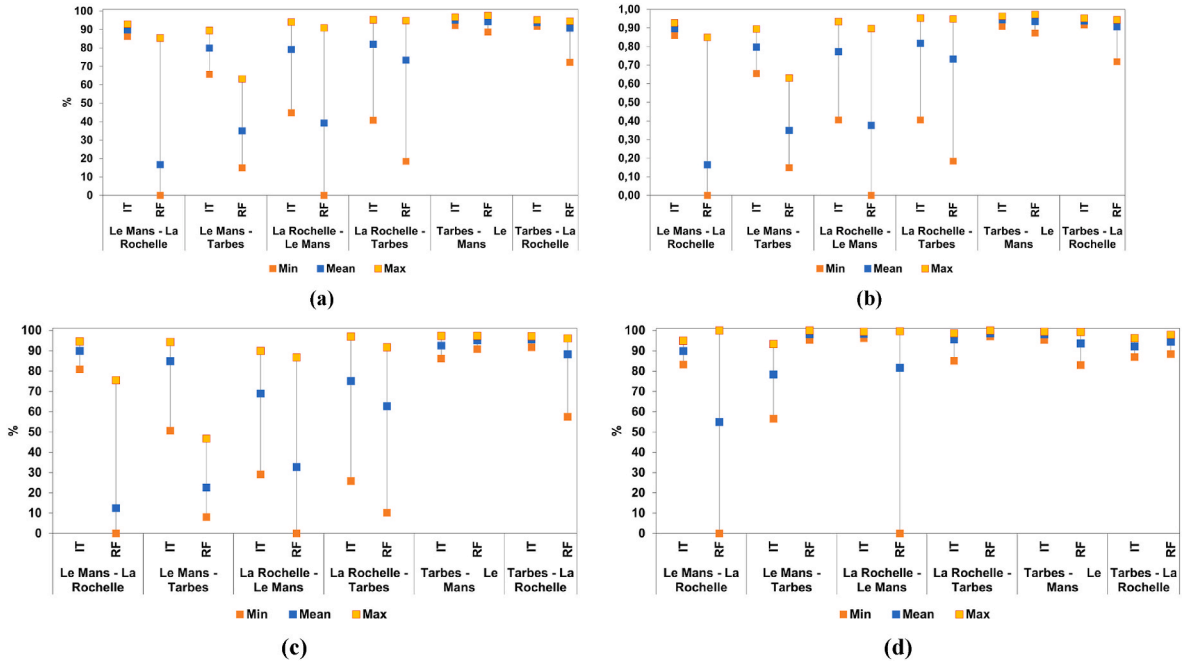

Fig. 12. Accuracy assessment for inception time (IT) and random forest (RF) using the unaligned S1 GDD series: (a) F1-Score, (b) Kappa, (c) Recall, (d) Precision. 'Mean' represents the average, 'Max' represents the highest value, and 'Min' represents the lowest value of each metric across the possible combinations of sites and years (9 combinations for each couple of datasets).

that for the unaligned data, IT outperforms RF, with higher F1-scores (89.2 % vs. 81.3 %) and a lower standard deviation (5.7 % vs. 16.5 %). Meaning that IT is better adapted to handle the possible shifts in the time series. After alignment, both RF and IT showed an improvement in F-scores (9 % for RF and 2.5 % for IT) and in standard deviation (8.3 % for RF and 1.9 % for IT). Meaning that our proposed alignment method helped the classifiers overcome the shifts in the rapeseed growth stages between different datasets. Furthermore, after alignment, both RF and IT had very close overall F1-scores (IT is better by around 1.4 % overall). However, the standard deviation of F1-scores shows that IT gives good results more consistently when compared with RF, with a difference of 10.8 % before alignment and 4.4 % after alignment.

For the unaligned S1 GDD series, IT greatly outperforms RF, with higher F1-scores (28.4 % difference) as well as a much lower standard

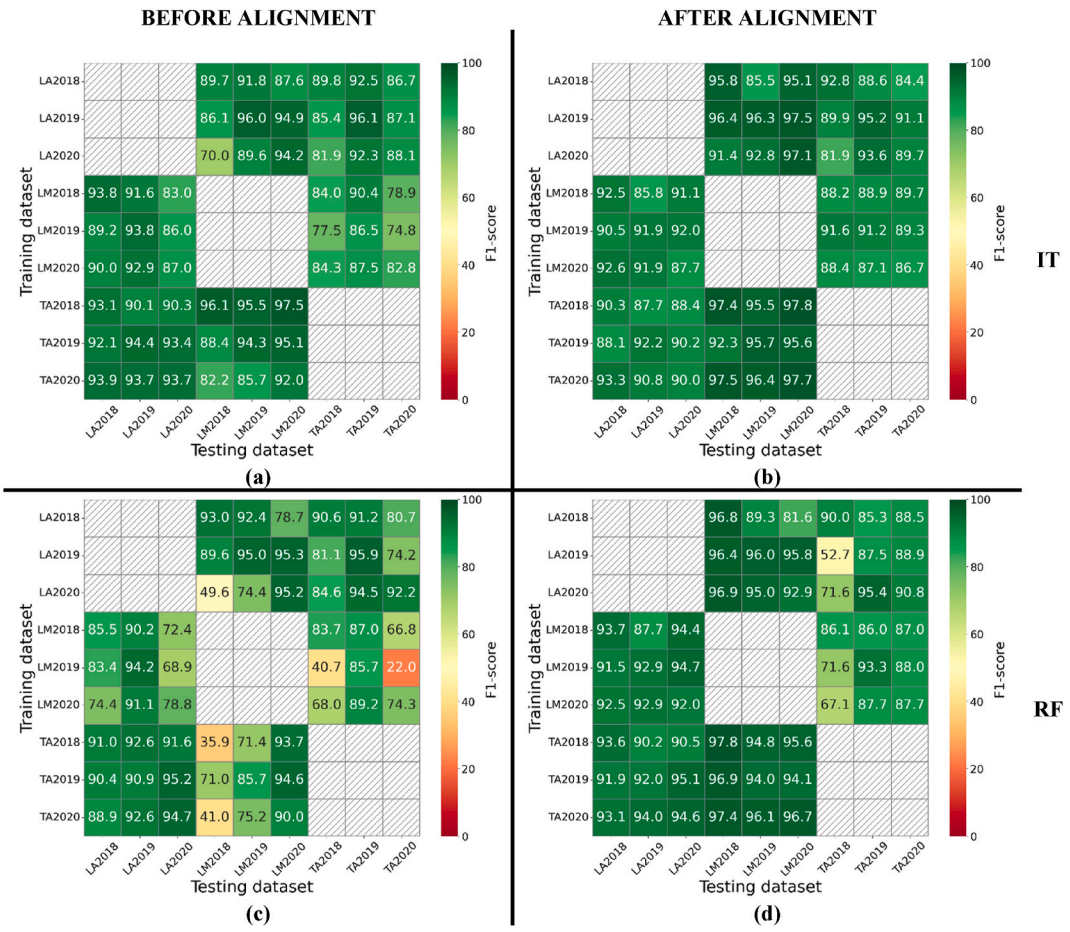

Fig. 13. F1-scores for all possible combinations in the spatiotemporal transfer scenario for S1 time series (a) IT before alignment, (b) IT after alignment, (c) RF before alignment, (d) RF after alignment.

deviation (11.7 % vs. 36.7 %). After alignment, there is no significant improvement in the overall F1-scores for IT. Nevertheless, there is an improvement of 1.4 % in the standard deviation. For RF, we observe an increase of 15.7 % in the overall F1-score and a 7.8 % improvement in terms of standard deviation before and after alignment. However, RF is still significantly outperformed by IT, with a difference of 12.7 % in F1-scores and 18.7 % between their respective standard deviations. This means that when using the S1 GDD series, alignment does not greatly impact the behavior of IT, whereas we can see a clear benefit for RF.

Comparing the S1 time series and the S1 GDD series shows that the S1 time series performs better, with an overall difference in the F1-score of 16.4 % for RF and 4.9 % for IT. The standard deviation of F1-scores between S1 time series were lower than those of S1 GDD series, with a difference of 20.8 % for RF and 6.5 % for IT. This indicates that in the case of spatiotemporal transfer, the S1 time series gives generally better results.

4.6. Rapeseed mapping

In this paper, we aim to rapeseed mapping method using S1 and GDD data. Crop mapping can be a very important tool for future agricultural management. This information can be used in the context of agricultural management in order to monitor and regulate farmland without the need for expensive field campaigns. We produced rapeseed maps using field boundary data from the RPG database. Fig. 15a represents the actual distribution of rapeseed fields over Le Mans in 2019. Fig. 15b shows the resulting rapeseed map over Le Mans in 2019 when using Tarbes 2020 at the training dataset and IT with aligned S1 time series (best performing pairing, with an F1-score of 91.9 %). Maps from all possible pairings of series (S1 time series/S1 GDD series), alignment (aligned/unaligned), and algorithm (IT/RF) are found in the appendix.

5. Discussion

In this work, we propose a rapeseed mapping method using Sentinel-1 SAR time series. Previous studies have explored rapeseed mapping using remote sensing data. For instance, some studies use optical remote sensing for rapeseed mapping, reporting F1-scores as high as 91.2 % (Han et al., 2021) and overall accuracies up to 98.8 % (Zhang et al., 2022). However, these optical methods are limited by cloud cover, which can result in incomplete rapeseed maps (Zhang et al., 2022). In contrast, our approach relies on Sentinel-1 SAR data, which is unaffected by atmospheric conditions, allowing for spatially consistent and continuous mapping.

Similar to our work, other studies have employed SAR data for rapeseed classification. Studies using Sentinel-1 time series data reported F1-scores ranging from 86 % to 91.7 % (Maleki et al., 2023). Furthermore, previous study by Saeideh et al. (Maleki et al., 2025), suggested an alignment technique to improve the spatial transfer performance based on detecting the rapeseed maximum peak growth present in the S1 time series, improving the classification performance by up to 45 %. Our results show comparable performance when using Sentinel-1 time series data, with F1-scores of 81.9 % (RF) and 89.2 % (IT) before alignment, increasing to 90.3 % and 91.7 % respectively after aligning the S1 time series using the flowering date as a reference point (McNairn et al., 2018, 2018d'Andrimont et al., 2020).

Concerning the classification timing (early mapping or late mapping), our method accomplishes rapeseed mapping during the month of

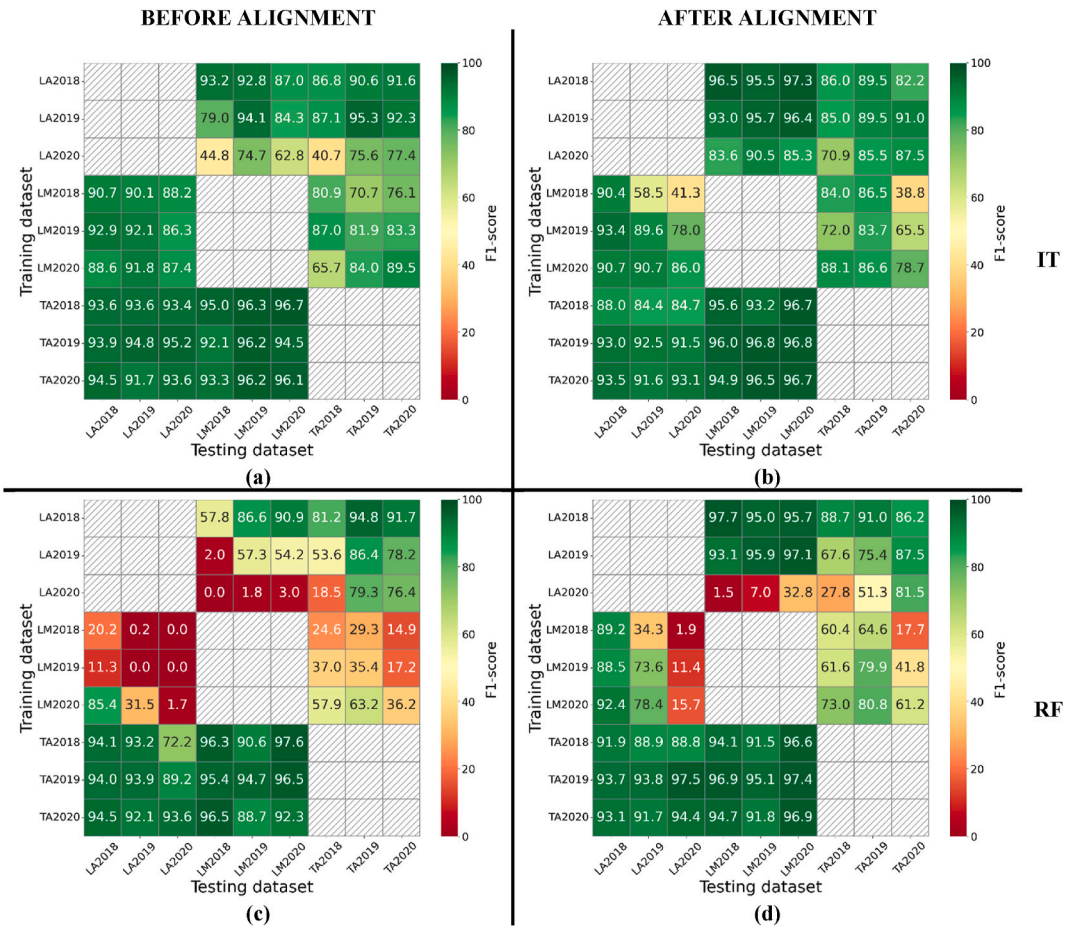

Fig. 14. F1-scores for all possible combinations in the spatiotemporal transfer scenario for S1 GDD series (a) IT before alignment, (b) IT after alignment, (c) RF before alignment, (d) RF after alignment.

Table 5
Mean F1-scores (in %) with standard deviation of RF and IT, using unaligned and aligned S1 time series and S1 GDD series.

	S1 time series		S1 GDD series	
	unaligned	aligned	unaligned	aligned
RF	81.3 ± 16.5	90.3 ± 8.2	58.2 ± 36.8	73.9 ± 29.0
IT	89.2 ± 5.7	91.7 ± 3.8	86.6 ± 11.7	86.8 ± 10.3

harvest (2 weeks before harvest at most depending on the region). More early mapping was not tested in this study because a previous study have shown that in the case of temporal transfer (different years used for training and testing), rapeseed mapping did not demonstrate good results, for early mapping, with accuracies below 50 %, when using time series spanning from September to March (Maleki et al., 2024). Moreover, Saeideh et al. (Maleki et al., 2024), assessed different time windows for rapeseed mapping using S1 time series, showing that at least a 5-month time series covering key growth stages such as stem elongation, inflorescence emergence, fruit development, and ending in the end of July, is required to achieve the highest detection accuracy (F1-scores >90 %).

Additionally, we investigated the use of growing degree days (GDD) in the form of Sentinel-1 GDD series. Currently, there are few works on crop mapping using remote sensing in tandem with GDD information. Shakun et al. (Skakun et al., 2017) used optical remote sensing and GDD for winter crop mapping with average coefficient of determination of $R^2 > 0.85$. In contrast, our findings showed that the GDD information is not always effective for better classification accuracies where the mapping precision did not significantly improve our classification results, showing lower overall F1-score compared to the use of the S1 time series data.

5.1. *Effect of starting date on S1 GDD series*

Like for all other crop types, the sowing date is generally used as the starting date for thermal time calculation for rapeseed (Šidlauskas et al., 2015; Kayacetin et al., 2019). However, with the exact sowing dates being usually unavailable at field scale, the calculation of ΣGDD remains limited. In unaligned datasets, the beginning of September was used as the starting date for ΣGDD calculation for all sites and years. This increases the likelihood of misalignments in the S1 GDD series since the sowing date could vary across sites and years. During the month of September, average temperatures were between 20 °C and 25 °C, meaning that the resulting increase in ΣGDD during that month could vary between 200 °C.days and 300 °C.days. On the other hand, after alignment based on the flowering date (April), the starting date for the calculation of ΣGDD would be in the month of January, where the ΣGDD gained during this first month ranges between 80 °C.days and 150 °C.days. In general, colder months contribute less to ΣGDD than hotter ones as is the case during the period of vernilization, where temperature are usually below 7 °C and the GDD accumulation is minimal. Consequently, the biggest shifts in GDD would probably occur during the hottest period of the year. All that being said, since the unaligned data starts in September, it has a higher chance of accumulating shifts in GDD (longer period and hotter months), whereas for aligned datasets, the potential for shifting is lesser since they span over relatively colder months and over shorter periods.

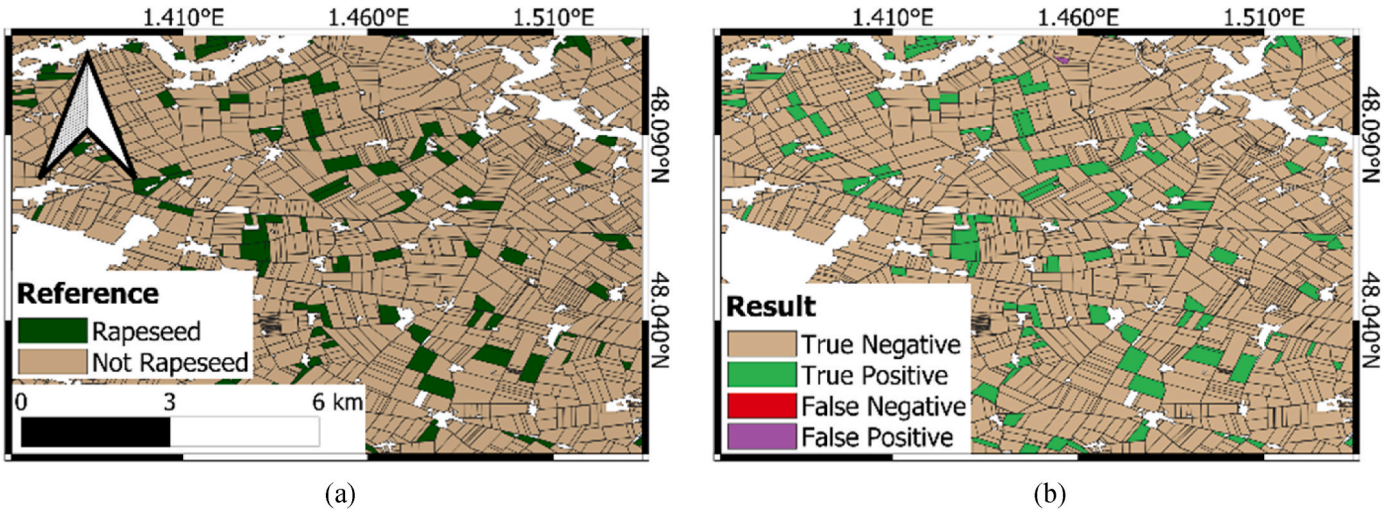

Fig. 15. Rapeseed maps in Le Mans (2019) dataset using Tarbes 2020 at the training dataset. (a) Reference rapeseed fields. (b) aligned S1 time series using IT.

Fig. 16a and b shows the S1 GDD series for two datasets (LM, 2019 and TB, 2020). Before and after alignment, respectively. In this combination, the shift between the S1 GDD series of these two datasets was the greatest. When using the unaligned datasets, the shift in GDD was about 300 °C.days, whereas for the aligned datasets, it was around 150 °C.days. This reduction in shift was positively reflected in the results, with the F1-scores of classification increasing from 17.2 % using RF and 83.3 % using IT for unaligned datasets to 80.8 % using RF and 86.6 % using IT after alignment. Therefore, starting ΣGDD calculation using inexact sowing dates could lead to uncertainty, making the alignment of time series necessary.

Additionally, since we are working on rapeseed in different climatic zones, it is likely to have different varieties of rapeseed in the different zones, with a varying temperature requirements. Hence, two given varieties could accumulate GDD differently regardless if they share the same sowing dates, this remains a challenge when employing S1 GDD series for rapeseed mapping.

5.2. *Effect of time shift on classification accuracy using S1 series*

The starting date for the aligned S1 time series was set to three months before the detected flowering date. Despite this alignment, some shifting in the S1 time series (between training and testing datasets) was observed in the pod formation and development phases (represented in the S1 time series as a great peak in VH polarization). Fig. 17a and b show the F1-score as a function of time shift (days) for IT and RF, respectively.

Fig. 17a shows that for IT, the classifier performance before alignment deteriorates when the time shift is 16 days or more, with the worst F1-score reaching 70.0 %. While for the aligned datasets, the time shift only slightly affected the performance, with an F1-score of 81.9 % for the worst performing pair of datasets with nine days of time shift. Fig. 17b shows that when employing RF, the F1-score decreases when the shift is six days or more for unaligned time series. The performance worsens as the time shift increases, reaching as low as around 20 % when the shift is 30 days (for one pair of datasets). On the other hand, for the aligned datasets, performance starts declining when the shift is more than 10 days, with the worst F1-scores reaching 52.7 % (one pair of datasets, time shift = 15 days). This means that alignment improved the results of RF by helping it overcome time shifts.

Generally, the performance of IT is less sensitive to time shifts compared to RF. This means that time shifts affect RF more than they do on IT, which is more robust to such time shifts.

5.3. *Effect of GDD shift on classification accuracy*

For the aligned S1 GDD series, 3 months were kept before the detected flowering date. During these periods, the evolution of ΣGDD is not similar for all the datasets; therefore, some shifting in the S1 GDD series persisted after alignment. Fig. 18a and b show the F1-score as a function of shift in ΣGDD (GDD) for RF and IT, respectively.

Fig. 18a shows that the performance of IT using aligned GDD series declines when the shift is greater than 200 °C.days, with the lowest F1-scores of 38.84 % having a shift of 225 °C.days. For the unaligned GDD series, the performance also starts to deteriorate when the shift in GDD exceeds 200 °C.days, with the lowest F1-score of 40.74 % for one pair of datasets at a GDD shift of 300 °C.days. Fig. 18b shows that for the aligned datasets, the degradation in performance begins when the shift is greater than 200 °C.days, with F1-scores reaching 1.53 % for one pair of datasets when the GDD shift is at its largest (300 °C.days). For

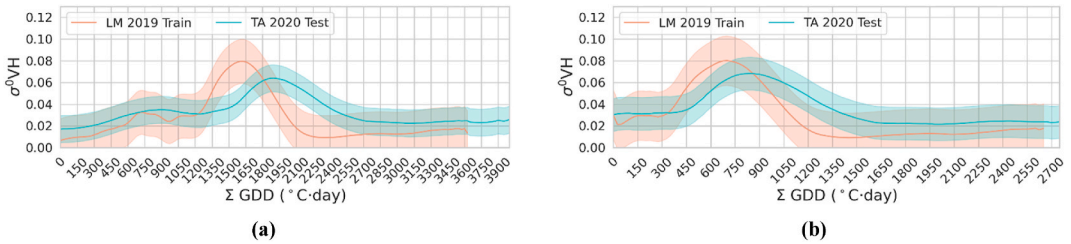

Fig. 16. S1 GDD series before (a) and after (b) alignment in VH polarization for the Tarbes 2020 and the Le Mans 2019 datasets. The shaded area corresponds to the standard deviation.

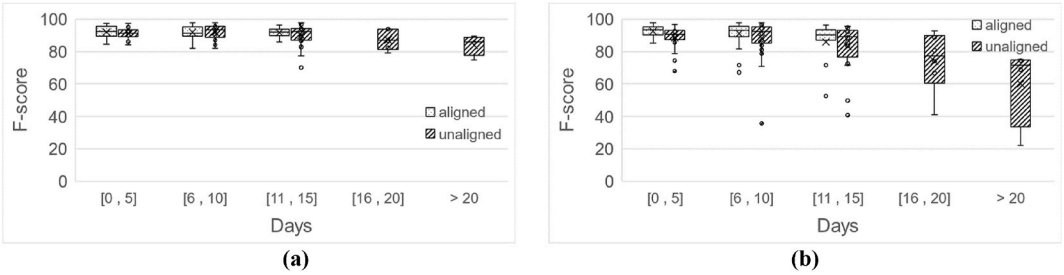

Fig. 17. F1-score as a function of time shift for (a) IT and (b) RF using the S1 time series.

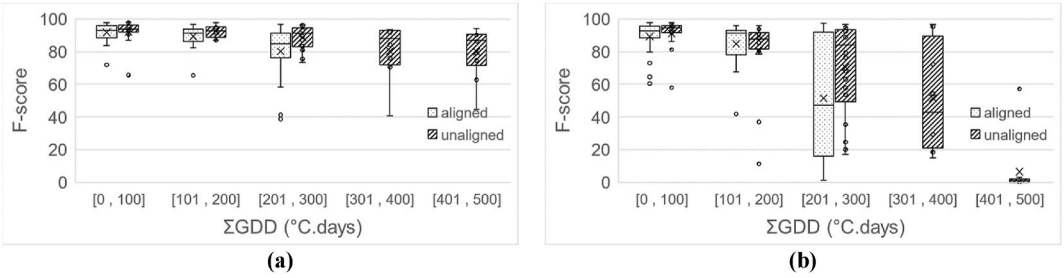

Fig. 18. F1-score as a function of shift in GDD for (a) IT and (b) RF using the S1 GDD series.

unaligned datasets, the performance of RF strongly degrades when the shift in GDD between training and testing exceeds 100 °C.days (reaching as low as 11.3 % at a shift of 175 °C.days), with the worst F1-scores reaching 0 % for multiple pairs of datasets when the shift in GDD is higher than 400 °C.days.

The degradation in performance is not as pronounced for IT as it is for RF (IT falls to around 40 %, whereas RF falls to 0 %). Showing that IT is more capable of overcoming shifts in GDD.

5.4. False positive analysis

False positive detections occur when a non-rapeseed field is classified as a rapeseed field. Using ground truth data, we can analyze the errors in our best-performing configuration over LM 2019 (aligned S1 times series using IT and with Tarbes, 2020 as the training dataset). Fig. 19 shows the distribution of crops most commonly misclassified as rapeseed fields. Analysis showed that 24.5 % of false positives were actually cabbage fields, followed by peas and barley at 16.3 % and 14.3 %, respectively.

The S1 time series for the crops that cause false positives is represented in Fig. 20. Fig. 20a shows the S1 time series in the VH polarization. We observe that in the months of May and June (rapeseed pod formation and seed development phases), other crops have similar peaks that are synchronous or partially synchronous with those of rapeseed. For example, during this period, we see a peak for cabbage that intersects partially with that of rapeseed and boasts the same amplitude of around 0.08 (−11.0 dB). Other crops, such as peas, barley, and alfalfa, have peaks that lie completely within the peak of rapeseed. However, their peak amplitudes do not exceed 0.05 (−13.0 dB). In the case of wheat, we do not see a significant peak coinciding with the signature rapeseed peak. Fig. 20b shows that in the VV polarization, there is a great intersection, throughout the growth cycle of rapeseed, between rapeseed and the other crops that were confused as such. The peak of cabbage intersects partially with that of rapeseed and has the same peak amplitude of 0.25 (−6.0 dB). Peas, barley, and alfalfa crops do show an increase in amplitude during the months of May and June, coinciding with the peak of rapeseed. However, none of them reached the same amplitude as rapeseed, with the highest one reaching around 0.12 (−9.2 dB), whereas rapeseed achieves 0.2 (−7.0 dB). When it comes to wheat, we can see that although it does not have a peak that coincides with that of rapeseed, its signal is highly similar to that of rapeseed in terms of shape and amplitude during the period that starts 1 January and ends at the end of March.

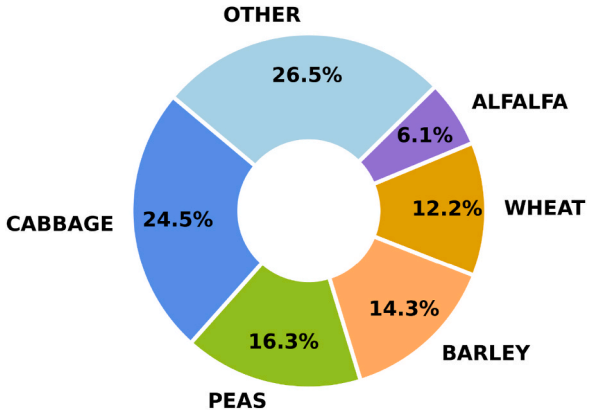

Fig. 19. The top crops comprising False Positives.

5.5. False negative analysis

False negatives occur when a rapeseed field is not classified as such (undetected rapeseed). Fig. 21a shows the average signal over detected rapeseed fields in LM 2019 as well as over fields where a false negative occurred when using IT, aligned S1 times series, and Tarbes 2020 as the training datasets. The average signal over detected rapeseed fields reaches 0.08 (−11 dB), much higher than that of false negative fields (0.05 = −13 dB) during the months of May and June (pod formation and seed development phase). This indicates that the classifier is sensitive to amplitude differences between training and testing datasets, as the false negatives have the expected rapeseed signal shape but with much lower peaks. Comparing the signal of these false negative fields with that of other crops in Fig. 20, we see that the signal for these false negative fields was in fact very similar to that of peas.

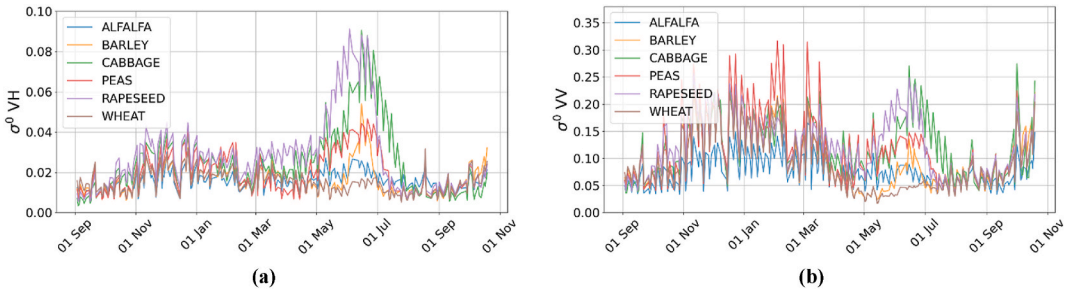

Fig. 20. S1 signal averages for the crops that were classified as rapeseed the most. (a) S1 time series in VH polarization. (b) S1 time series in VV polarization.

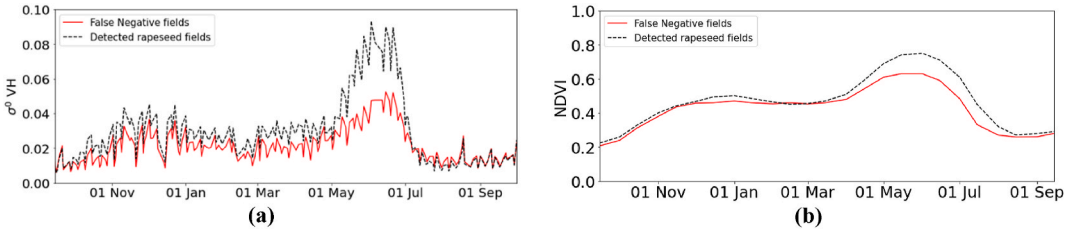

Fig. 21. (a) Average signal in VH polarization for detected rapeseed fields and for false negative fields. (b) Average NDVI for detected rapeseed fields and for false negative fields.

Fig. 21b shows the NDVI time series of true positive and false negative plots calculated using the Sentinel-2 data. The analysis of the NDVI time series in Fig. 21b shows that there is little difference in the peak NDVI between false negative fields and the detected rapeseed fields (around 0.1), meaning that the difference in the S1 signal in Fig. 21a is probably due to fewer pods being formed during this critical stage in the rapeseed cycle and consequently to rapeseed fields with lower yield.

6. Conclusion

This study evaluated S1 data for rapeseed mapping in the case of spatiotemporal generalization. It also assessed the coupling of S1 data with thermal time using a novel S1 GDD time series. An alignment applied to both the S1 and S1 GDD time series was proposed, aiming to alleviate the shifts between the different datasets (different sites and years). The classification of rapeseed was realized using two machine-learning models, namely, random forest (RF) and inception time (IT).

Before alignment, the results showed that IT outperformed RF for both the S1 time series and the S1 GDD series by a large margin, meaning that IT is better at overcoming shifts between the training and testing datasets. After alignment, the classification performance of RF improved greatly for both S1 time series and S1 GDD series, but its accuracy remained inferior to that of IT, which mainly showed an improvement in the consistency of good results for most pairs of datasets. Generally, using S1 time series brought about better results when compared to S1 GDD series, showing that for rapeseed mapping, S1 GDD series do not provide advantages over S1 time series. In fact, the best classification performance was obtained using aligned S1 times series and IT (F1-score $= 91.7 \pm 3.8$).

This suggested that modern mapping approach can reduce the need for repeated ground-truth campaigns, thus allowing for regular mapping of rapeseed across various sites and different years by using previously collected data as training data and the proposed alignment method. Regular mapping of rapeseed cultivation is valuable for both policymakers and stakeholders, as it enables more effective and timely monitoring of cultivated areas and agricultural production.

CRediT authorship contribution statement

Sami Najem: Writing – review & editing, Writing – original draft, Validation, Software, Methodology, Investigation, Formal analysis, Data curation. **Nicolas Baghdadi:** Writing – review & editing, Resources, Project administration, Methodology, Investigation, Funding acquisition, Formal analysis, Conceptualization. **Ya Gao:** Writing – review & editing, Software, Resources, Methodology, Data curation. **Hassan Bazzi:** Writing – review & editing, Validation. **Saeideh Maleki:** Writing – review & editing. **Cassio Fraga Dantas:** Writing – review & editing. **Dino Ienco:** Writing – review & editing.

Declaration of competing interest

The authors declare the following financial interests/personal relationships which may be considered as potential competing interests: Sami Najem reports financial support, administrative support, article publishing charges, and statistical analysis were provided by French National Institute for Agricultural Research INRAE. If there are other authors, they declare that they have no known competing financial interests or personal relationships that could have appeared to influence the work reported in this paper.

Acknowledgment

The authors would like to thank the French Space Study Center (CNES, TOSCA 2024), and the National Research Institute for Agriculture, Food and the Environment (INRAE) for their support in carrying out this research. We are also grateful to the European Space Agency (ESA) for providing the S1 images.

Appendix

Fig. 22 shows the S1 GDD series of the most common crops in our study sites.

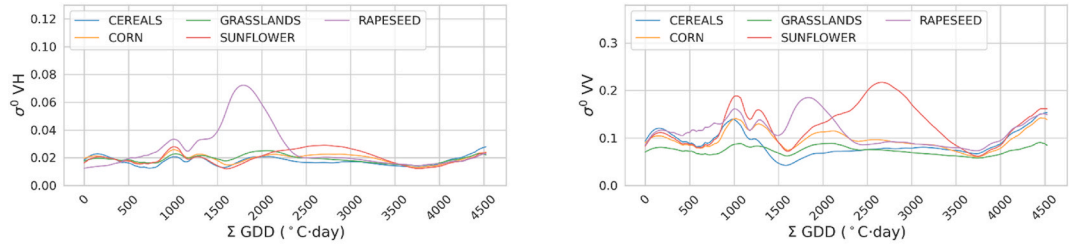

Fig. 22. S1 GDD series according to the cumulative GDD (ΣGDD in GDD) showing the main crops in La Rochelle (2018) dataset.

Fig. 23 represents the accuracy metrics for the transferability of IT and RF classifiers.

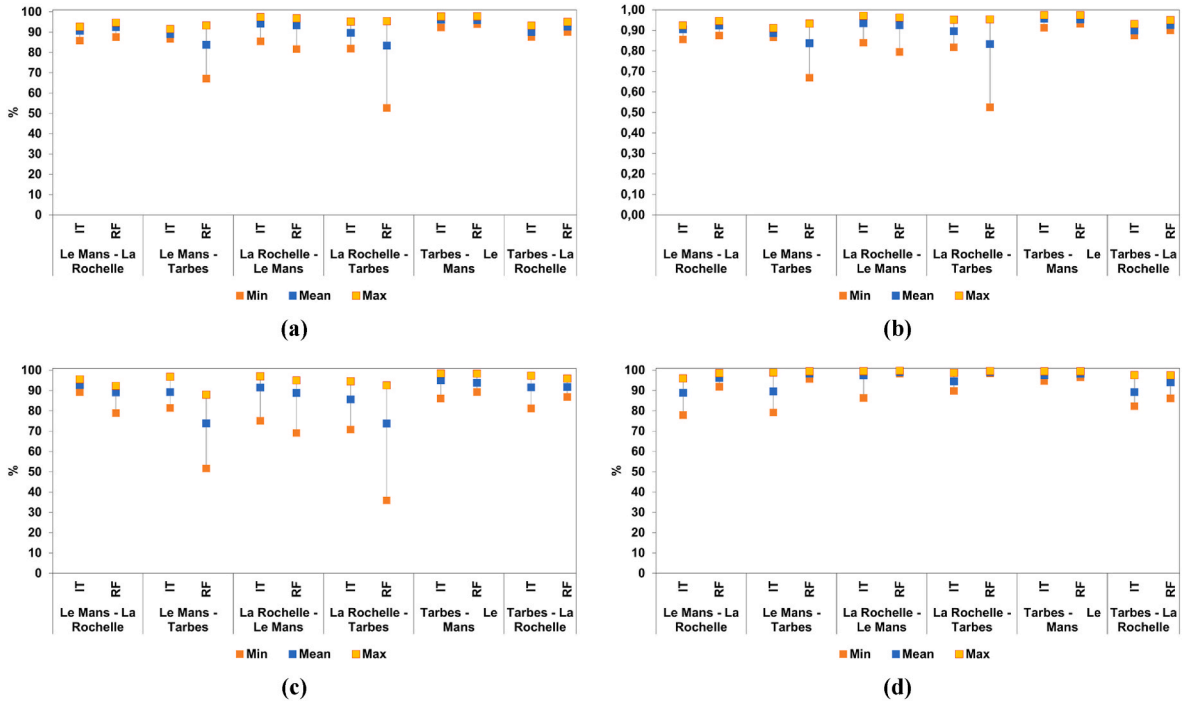

Fig. 23. Accuracy assessment for inception time (IT) and random forest (RF) using the aligned S1 times series (different site and year for training and testing): (a) F1-Score, (b) Kappa, (c) Recall, (d) Precision. 'Mean' represents the average, 'Max' represents the highest value and 'Min' represents the lowest value of each metric across the possible combinations of sites and years (9 combinations for each couple of datasets).

Fig. 24 represents the accuracy metrics for the transferability of IT and RF classifiers.

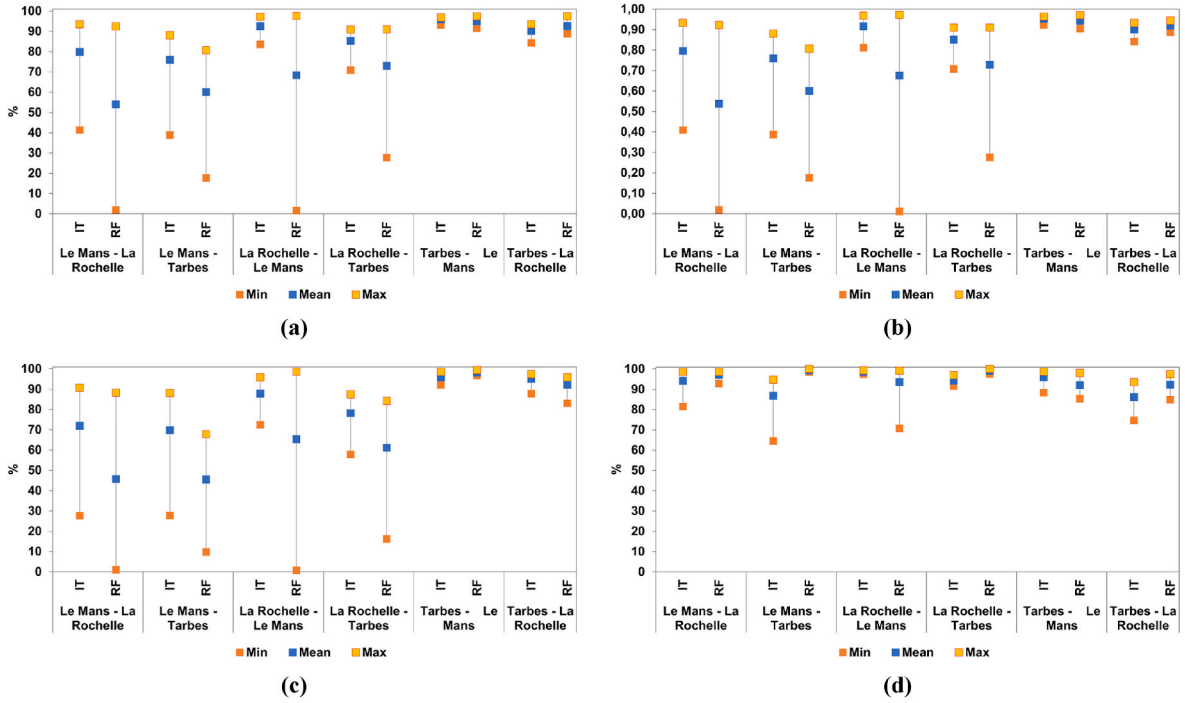

Fig. 24. Accuracy assessment for inception time (IT) and random forest (RF) using the aligned S1 GDD series (different site and year for training and testing): (a) F1-Score, (b) Kappa, (c) Recall, (d) Precision. 'Mean' represents the average, 'Max' represents the highest value and 'Min' represents the lowest value of each metric across the possible combinations of sites and years (9 combinations for each couple of datasets).

Fig. 25 represents maps of a section over the Le Mans dataset in 2019, using training data from Tarbes (2020) for all possible pairings of series (S1 time series/S1 GDD series), alignment (aligned/unaligned), and algorithm (IT/RF), as opposed to only the best performing combination found in Fig. 15. Fig. 25a shows the reference rapeseed fields data, and Fig. 25b–i show the rapeseed mapping results.

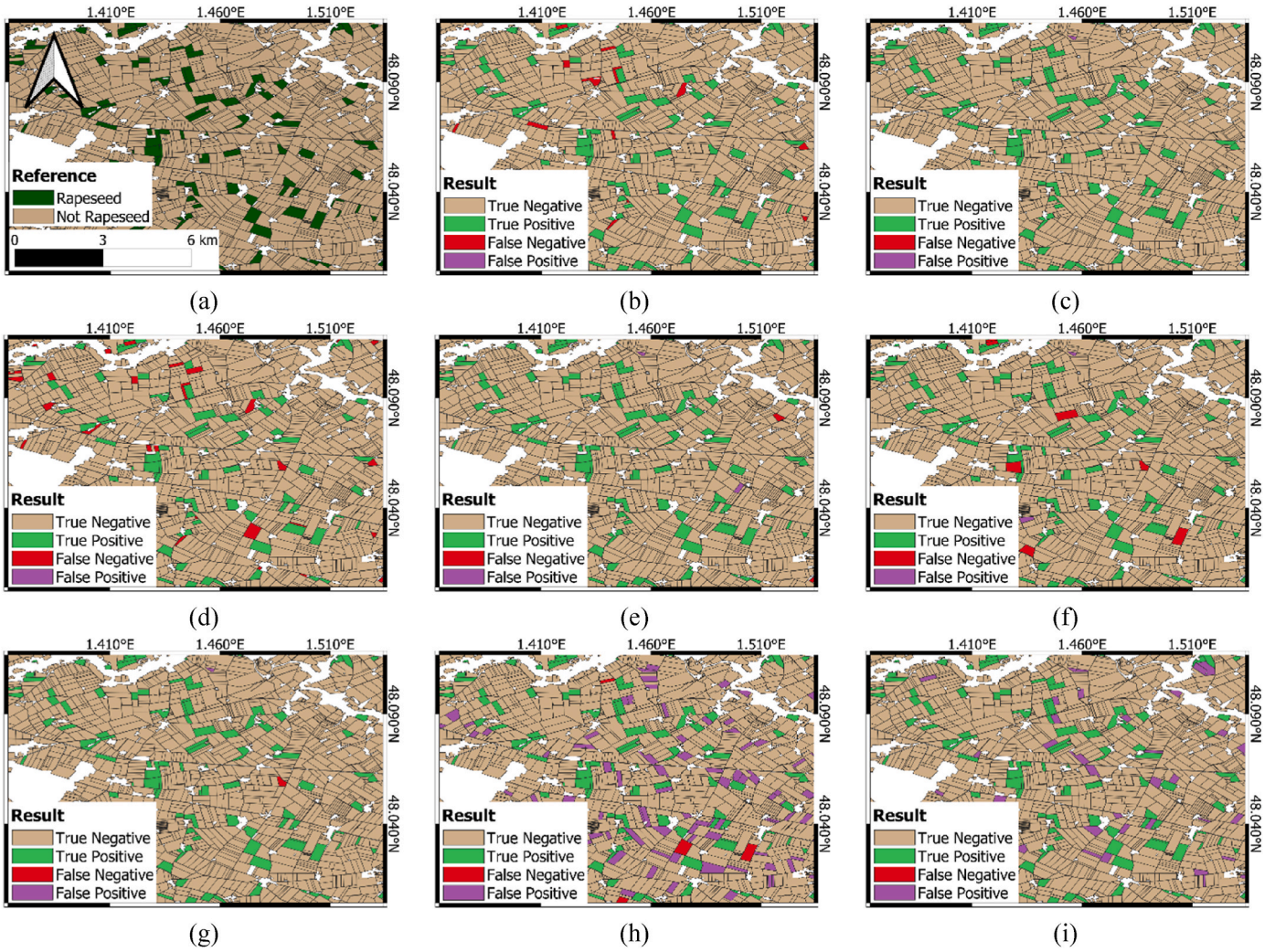

Fig. 25. Rapeseed maps in Le Mans (2019) dataset using Tarbes 2020 at the training dataset. (a) Reference rapeseed fields. (b) unaligned S1 time series using IT. (c) aligned S1 time series using IT. (d) unaligned S1 time series using RF. (e) aligned S1 time series using RF. (f) unaligned S1 GDD series using IT. (g) aligned S1 GDD series using IT. (h) unaligned S1 GDD series using RF. (i) aligned S1 GDD series using RF.

Data availability

Data will be made available on request.

References

Addabbo, P., Focareta, M., Marcuccio, S., Votto, C., Ullo, S.L., 2016. Contribution of sentinel-2 data for applications in vegetation monitoring. Acta Imeko 5, 44–54.

Akhter, M.T., Mannan, M.A., Kundu, P.B., Paul, N.K., 2015. Effects of different sowing dates on the phenology and accumulated heat units in three rapeseed (Brassica campestris L.) varieties. Bangladesh J. Bot. 44, 97–101.

Amani, M., Ghorbanian, A., Ahmadi, S.A., Kakooei, M., Moghimi, A., Mirmazloumi, S.M., Moghaddam, S.H.A., Mahdavi, S., Ghahremanloo, M., Parsian, S., 2020. Google earth engine cloud computing platform for remote sensing big data applications: a comprehensive review. IEEE J. Sel. Top. Appl. Earth Obs. Rem. Sens. 13, 5326–5350.

Aschbacher, J., Ofren, R., Delsol, J.P., Suselo, T.B., Vibulsresth, S., Charrupat, T., 1995. An integrated comparative approach to mangrove vegetation mapping using advanced remote sensing and GIS technologies: preliminary results. Hydrobiologia (The Hague) 295, 285–294.

Ashourloo, D., Shahrabi, H.S., Azadbakht, M., Aghighi, H., Nematollahi, H., Alimohammadi, A., Matkan, A.A., 2019. Automatic canola mapping using time series of Sentinel 2 images. ISPRS J. Photogrammetry Remote Sens. 156, 63–76.

Atwell, B.J., 1999. Plants in action: adaptation in nature. Performance in Cultivation. Macmillan Education AU. ISBN 978-0-7329-4439-1.

Bajželj, B., Richards, K.S., Allwood, J.M., Smith, P., Dennis, J.S., Curmi, E., Gilligan, C.A., 2014. Importance of food-demand management for climate mitigation. Nat. Clim. Change 4, 924–929.

Betbeder, J., Rapinel, S., Corpetti, T., Pottier, E., Corgne, S., Hubert-Moy, L., 2014. Multitemporal classification of TerraSAR-X data for wetland vegetation mapping. JARS 8, 083648. https://doi.org/10.1117/1.JRS.8.083648.

Bindraban, P.S., van der Velde, M., Ye, L., Van den Berg, M., Materechera, S., Kiba, D.I., Tamene, L., Ragnarsdóttir, K.V., Jongschaap, R., Hoogmoed, M., 2012. Assessing the impact of soil degradation on food production. Curr. Opin. Environ. Sustain. 4, 478–488.

Choudhury, I., Chakraborty, M., 2006. SAR signature investigation of rice crop using RADARSAT data. Int. J. Rem. Sens. 27, 519–534.

Dong, J., Xiao, X., Menarguez, M.A., Zhang, G., Qin, Y., Thau, D., Biradar, C., Moore III, B., 2016. Mapping paddy rice planting area in northeastern asia with landsat 8 images, phenology-based algorithm and Google earth engine. Rem. Sens. Environ. 185, 142–154.

d'Andrimont, R., Taymans, M., Lemoine, G., Ceglar, A., Yordanov, M., van der Velde, M., 2020. Detecting flowering phenology in oil seed rape parcels with sentinel-1 and -2 time series. Rem. Sens. Environ. 239, 111660. https://doi.org/10.1016/j.rse.2020.111660.

Friedt, W., Tu, J., Fu, T., 2018. Academic and economic importance of Brassica napus rapeseed. In: Liu, S., Snowdon, R., Chalhoub, B. (Eds.), The Brassica Napus Genome. Springer International Publishing, Cham, pp. 1–20. ISBN 978-3-319-43694-4.

Girault, A., 1973. The study of some properties of rapeseed protein with a view to protein concentrate production. J. Sci. Food Agric. 24, 509–518.

Han, J., Zhang, Z., Luo, Y., Cao, J., Zhang, L., Zhang, J., Li, Z., 2021. The RapeseedMap10 database: annual maps of rapeseed at a spatial resolution of 10 m based on multi-source data. Earth Syst. Sci. Data 13, 2857–2874.

Hussain, S., Gao, K., Din, M., Gao, Y., Shi, Z., Wang, S., 2020. Assessment of UAV-onboard multispectral sensor for non-destructive site-specific rapeseed crop phenotype variable at different phenological stages and resolutions. Remote Sens. 12, 397. https://doi.org/10.3390/rs12030397.

Inglada, J., Arias, M., Tardy, B., Hagolle, O., Valero, S., Morin, D., Dedieu, G., Sepulcre, G., Bontemps, S., Defourny, P., 2015. Assessment of an operational system for crop type map production using high temporal and spatial resolution satellite optical imagery. Remote Sens. 7, 12356–12379.

Ismail Fawaz, H., Lucas, B., Forestier, G., Pelletier, C., Schmidt, D.F., Weber, J., Webb, G. I., Idoumghar, L., Muller, P.-A., Petitjean, F., 2020. Inceptiontime: finding alexnet for time series classification. Data Min. Knowl. Discov. 34, 1936–1962.

Jiao, X., McNairn, H., Shang, J., Liu, J., 2010. The sensitivity of multi-frequency (X, C and L-band) radar backscatter signatures to bio-physical variables (LAI) over corn and soybean fields. Intern. Arch. Photogram. Remote Sens. Spatial Inform. Sci. - ISPRS Archives 38, 317–321.

Kaleem, S., Hassan, F., Saleem, A., 2009. Influence of environmental variations on physiological attributes of sunflower. Afr. J. Biotechnol. 8.

Kayacetin, F., Önemli, F., Yilmaz, G., Khawar, K.M., Kinay, A., Hatipoğlu, H., Kivilcim, M.N., Nimet, K., Arzu, K., Sefaoğlu, F., 2019. Growing degree day and seed yield relationships in mustard (Brassica juncea L.) under different sowing seasons and locations of Turkey. J. Agric. Sci. 25, 298–308.

Kumar, P., Prasad, R., Gupta, D.K., Mishra, V.N., Vishwakarma, A.K., Yadav, V.P., Bala, R., Choudhary, A., Avtar, R., 2018. Estimation of winter wheat crop growth parameters using time series sentinel-1A SAR data. Geocarto Int. 33, 942–956.

Lampropoulos, G., Li, Y., Liu, T., 2015. Advancements in estimating crop growth stages using RADARSAT-2 and TerraSAR-X polarimetric data. Int. Arch. Photogram. Rem. Sens. Spatial Inf. Sci. 40, 1227–1232.

Liu, W., Li, S., Tao, J., Liu, X., Yin, G., Xia, Y., Wang, T., Zhang, H., 2024. CARM30: China annual rapeseed maps at 30 m spatial resolution from 2000 to 2022 using multi-source data. Sci. Data 11, 356.

Luo, Y., Zhang, Z., Zhang, L., Han, J., Cao, J., Zhang, J., 2022. Developing high-resolution crop maps for major crops in the European union based on transductive transfer learning and limited ground data. Remote Sens. 14, 1809.

Luo Tao, L.T., Xian MengZhu, X.M., Khan, M.N., Hu LiYong, H.L., Xu ZhengHua, X.Z., 2018. Estimation of Base Temperature for Germination of Rapeseed (Brassica Napus) Using Different Models.

Maleki, S., Baghdadi, N., Dantas, C.F., Najem, S., Bazzi, H., Reluy, N.P., Ienco, D., Zribi, M., 2023. Artificial intelligence algorithms for rapeseed fields mapping using sentinel-1 time series: temporal transfer scenario and ground sampling constraints. IEEE J. Sel. Top. Appl. Earth Obs. Rem. Sens. 16, 8884–8899. https://doi.org/10.1109/JSTARS.2023.3316304.

Maleki, S., Baghdadi, N., Najem, S., Dantas, C.F., Bazzi, H., Ienco, D., 2024. Determining effective temporal windows for rapeseed detection using sentinel-1 time series and machine learning algorithms. Remote Sens. 16, 549.

Maleki, S., Baghdadi, N., Najem, S., Dantas, C.F., Ienco, D., Bazzi, H., 2025. Sentinel-1 (S1) time series alignment method for rapeseed fields mapping. Front. Remote Sens. 5, 1483295. https://doi.org/10.3389/frsen.2024.1483295.

McNairn, H., Shang, J., 2016. A review of multitemporal synthetic aperture radar (SAR) for crop monitoring. Multitemp. Remote Sens.: Methods Applic. 317–340.

McNairn, H., Jiao, X., Pacheco, A., Sinha, A., Tan, W., Li, Y., 2018. Estimating canola phenology using synthetic aperture radar. Rem. Sens. Environ. 219, 196–205. https://doi.org/10.1016/j.rse.2018.10.012.

Meng, S., Zhong, Y., Luo, C., Hu, X., Wang, X., Huang, S., 2020. Optimal temporal window selection for winter wheat and rapeseed mapping with sentinel-2 images: a case study of zhongxiang in China. Remote Sens. 12, 226.

Meyfroidt, P., 2018. Trade-offs between environment and livelihoods: bridging the global land use and food security discussions. Global Food Secur. 16, 9–16.

Mittaine, J.-F., Mielke, T., 2012. The globalization of international oilseeds trade. OCL 19, 249–260. https://doi.org/10.1051/ocl.2012.0470.

Mulla, D.J., 2013. Twenty five years of remote sensing in precision agriculture: key advances and remaining knowledge gaps. Biosyst. Eng. 114, 358–371. https://doi.org/10.1016/j.biosystemseng.2012.08.009.

Najem, S., Baghdadi, N., Bazzi, H., Lalande, N., Bouchet, L., 2023. Detection and mapping of cover crops using sentinel-1 SAR remote sensing data. IEEE J. Sel. Top. Appl. Earth Obs. Rem. Sens. https://doi.org/10.1109/JSTARS.2023.3337989.

Nasrallah, A., Baghdadi, N., El Hajj, M., Darwish, T., Belhouchette, H., Faour, G., Darwich, S., Mhawej, M., 2019. Sentinel-1 data for winter wheat phenology monitoring and mapping. Remote Sens. 11. https://doi.org/10.3390/rs11192228.

Navascues, B.; Ayuso, J.J.; Jarvenoja, S. Analysis of Surface Variables and Parameterization of Surface Processes in HIRLAM. Part I: Approach and Verification by Parallel Runs.

Neetu, Ray, S.S., 2019. Exploring machine learning classification algorithms for crop classification using Sentinel 2 data. Int. Arch. Photogram. Rem. Sens. Spatial Inf. Sci. 42, 573–578.

Neild, R.E., Newman, J.E., 1987. *Growing Season Characteristics And Requirements In the Corn Belt*; Cooperative Extension Service. Iowa State University.

Nguyen, D.B., Wagner, W., 2017. European rice cropland mapping with sentinel-1 data: the mediterranean region case study. Water (Lond. 1974) 9, 392.

Nwogha, J.S., 2014. The Effect of Temperature on Phenological Responses and Growth of Canola Cultivars. Stellenbosch University, Stellenbosch.

Oilseeds, U.S.D.A., 2023. World markets and trade. Foreign Agricul. Serv./Global Market Analy. 2023.

Qadir, A., Mondal, P., 2020. Synergistic use of radar and optical satellite data for improved monsoon cropland mapping in India. Remote Sens. 12, 522.

Qadir, G., Fayyaz-ul-Hassan, Malik, M.A., 2007. Growing degree days and yield relationship in sunflower (helianthus annuus L.). Int. J. Agric. Biol. 9.

Qian, Y., Yang, Z., Di, L., Rahman, M.S., Tan, Z., Xue, L., Gao, F., Yu, E.G., Zhang, X., 2019. Crop growth condition assessment at county scale based on heat-aligned growth stages. Remote Sens. 11, 2439. https://doi.org/10.3390/rs11202439.

Quintana Seguí, P., Peral García, M.C., Turco, M., Llasat, M. del C., Martin, E., 2016. Meteorological Analysis Systems in North-East Spain: Validation of SAFRAN and SPAN.

Remote sensing of land Resources: monitoring, modeling, and mapping advances over the last 50 Years and a vision for the future. In: Remote Sensing Handbook - Three Volume Set, 2015. CRC Press. ISBN 978-0-429-18819-0.

Rondanini, D.P., Gomez, N.V., Agosti, M.B., Miralles, D.J., 2012. Global trends of rapeseed grain yield stability and rapeseed-to-wheat yield ratio in the last four decades. Eur. J. Agron. 37, 56–65. https://doi.org/10.1016/j.eja.2011.10.005.

Shaykewich, C.f., Bullock, P.r., 2020. Modeling canola phenology. In: Agroclimatology. John Wiley & Sons, Ltd, pp. 303–325. ISBN 978-0-89118-358-7.

Šidlauskas, G., Pranckietienė, I., Dromantienė, R., Pranckietis, V., 2015. The effect of agronomic and climatic factors on winter oilseed rape (BRASSICA napus L.) root neck growth in autumn. International Scientific Conference RURAL DEVELOPMENT 2017.

Skakun, S., Franch, B., Vermote, E., Roger, J.-C., Becker-Reshef, I., Justice, C., Kussul, N., 2017. Early season large-area winter crop mapping using MODIS NDVI data, growing degree days information and a Gaussian mixture model. Rem. Sens. Environ. 195, 244–258. https://doi.org/10.1016/j.rse.2017.04.026.

Tao, J., Wu, W., Yong, Z., Yu, W., Jiang, Y., 2017. Mapping winter wheat using phenological feature of peak before winter on the north China plain based on time-series MODIS data. J. Integr. Agric. 16, 348–359.

Tian, H., Chen, T., Li, Q., Mei, Q., Wang, S., Yang, M., Wang, Y., Qin, Y., 2022. A novel spectral index for automatic canola mapping by using sentinel-2 imagery. Remote Sens. 14, 1113. https://doi.org/10.3390/rs14051113.

Van Duren, I., Voinov, A., Arodudu, O., Firrisa, M.T., 2015. Where to produce rapeseed biodiesel and why? Mapping European rapeseed energy efficiency. Renew. Energy 74, 49–59.

Vigil, M.F., Anderson, R.L., Beard, W.E., 1997. Base temperature and growing-degree-hour requirements for the emergence of canola. Crop Sci. 37. https://doi.org/10.2135/cropsci1997.0011183X003700030025x cropsci1997.0011183X003700030025x.

Vreugdenhil, M., Wagner, W., Bauer-Marschallinger, B., Pfeil, I., Teubner, I., Rüdiger, C., Strauss, P., 2018. Sensitivity of sentinel-1 backscatter to vegetation dynamics: an Austrian case study. Remote Sens. 10, 1396. https://doi.org/10.3390/rs10091396.

Wei, X., Chang, N.-B., Bai, K., Gao, W., 2020. Satellite remote sensing of aerosol optical depth: advances, challenges, and perspectives. Crit. Rev. Environ. Sci. Technol. 50, 1640–1725.

Whitcraft, A.K., Vermote, E.F., Becker-Reshef, I., Justice, C.O., 2015. Cloud cover throughout the agricultural growing season: impacts on passive optical earth observations. Rem. Sens. Environ. 156, 438–447.

Zhang, W., Chen, E., Li, Z., Zhao, L., Ji, Y., Zhang, Y., Liu, Z. Rape, Brassica, Napus L., 2018. Growth monitoring and mapping based on radarsat-2 time-series data. Remote Sens. 10, 206. https://doi.org/10.3390/rs10020206.

Zhang, H., Liu, W., Zhang, L., 2022. Seamless and automated rapeseed mapping for large cloudy regions using time-series optical satellite imagery. ISPRS J. Photogrammetry Remote Sens. 184, 45–62. https://doi.org/10.1016/j.isprsjprs.2021.12.001.

Zhao, H., Chen, Z., Jiang, H., Jing, W., Sun, L., Feng, M., 2019. Evaluation of three deep learning models for early crop classification using sentinel-1A imagery time series—a case study in zhanjiang, China. Remote Sens. 11, 2673.

Zhao, L., Wang, S., Xu, Y., Sun, W., Shi, L., Yang, J., Dash, J., 2023. Evaluating the capability of sentinel-1 data in the classification of canola and wheat at different growth stages and in different years. Remote Sens. 15, 2731. https://doi.org/10.3390/rs15112731.